

# Paraventricular hypothalamic input to anterior cingulate cortex controls food preferences in chronic visceral pain mice

Received: 27 August 2024

Accepted: 12 June 2025

Published online: 01 July 2025



Qi-Ya Xu<sup>1,2,6</sup>, Ying Kong<sup>3,6</sup>, Xiao-Wen Meng<sup>1,2</sup>, Ke Peng<sup>1,2</sup>, Yang Yu<sup>4</sup>,  
Shao-Yong Song<sup>1</sup>, Yu-Fan Yang<sup>1,2</sup>, Hua-Yue Liu<sup>1,2,5</sup> , Guang-Yin Xu<sup>4</sup>  &  
Fu-Hai Ji<sup>1,2</sup> 

Chronic visceral pain is frequently accompanied by changes in food preference. The paraventricular hypothalamus (PVH) and the anterior cingulate cortex (ACC) are well-known regions involved in pain processing and food intake. However, the underlying neural circuitry mechanisms remain unclear. Here, we showed that a circuit from cholecystokinin neurons in the PVH (PVH<sup>CCK</sup>) projecting to glutamatergic neurons in the ACC (ACC<sup>Glu</sup>) to regulate food preference in male mice with chronic visceral pain induced by neonatal colonic inflammation (NCI). The mice with chronic visceral pain preferred for sucrose when compared with control mice. Chemogenetic inhibition of the PVH<sup>CCK</sup> to ACC<sup>Glu</sup> circuit reduced chronic visceral pain and led to food preference switched from sucrose to intralipid, which was reversed by an injection of an agonist of CCKBRs in the ACC. Chemogenetic activation of PVH<sup>CCK</sup> to ACC<sup>Glu</sup> circuit increased visceral pain and resulted in food preference switched from intralipid to sucrose, which was reversed by an injection of an antagonist of cholecystokinin receptors (CCKBRs) in the ACC. Our study indicates that the PVH<sup>CCK</sup> to ACC<sup>Glu</sup> circuit encodes changes in food preference during chronic visceral pain. Intervention targeting this neural circuitry might be a potential therapeutic strategy for patients with chronic visceral pain.

Chronic pain affects up to 20% of the global population and presents a significant therapeutic challenge<sup>1</sup>. Chronic pain is known to impact feeding behavior<sup>2</sup> and eating disorders may aggravating pain<sup>3</sup>. Furthermore, eating disorders may increase incidence of mental disorders and suicide high-risk in patients<sup>4</sup>. However, mechanism underlying the feedback between chronic pain and feeding behaviors remains largely unknown. Current treatments are mainly by following the principles of a healthy diet, the physiological homeostasis can be managed, as well as faster recovery from disease achieved<sup>5</sup>. Although dietary therapies are

rapidly becoming first-line treatment of chronic visceral pain, negative effects and warning symptoms of poor eating patterns can also occur. Therefore, it is important to expound the mechanisms of food preference and to provide a therapeutic directions and theoretical basis for pain management. Here, a mouse model induced by neonatal colonic inflammation (NCI) was used, as NCI has been shown to induce chronic visceral pain in adult rats and mice<sup>6,7</sup>. Overall, the aim of this study was to explore the neural circuitry underlying changes in food preference associated with chronic visceral pain in an NCI mouse model.

<sup>1</sup>Department of Anesthesiology, The First Affiliated Hospital of Soochow University, Suzhou 215006, China. <sup>2</sup>Institute of Anesthesiology, Soochow University, Suzhou 215006, China. <sup>3</sup>Department of Urology, The First Affiliated Hospital of Soochow University, Suzhou 215000, China. <sup>4</sup>Jiangsu Key Laboratory of Neuropsychiatric Diseases, Institute of Neuroscience, Soochow University, Suzhou 215123, China. <sup>5</sup>Ambulatory Surgery Center, The First Affiliated Hospital of Soochow University, Suzhou 215006, China. <sup>6</sup>These authors contributed equally: Qi-Ya Xu, Ying Kong. ✉ e-mail: [docliu.hy@163.com](mailto:docliu.hy@163.com); [guangyinxu@suda.edu.cn](mailto:guangyinxu@suda.edu.cn); [jifuhaisuda@163.com](mailto:jifuhaisuda@163.com)

Some several brain regions involved in the modulation of pain processing, including the claustrum (CL)<sup>8</sup>, paraventricular thalamus (PVT)<sup>9</sup>, anterior cingulate cortex (ACC)<sup>10,11</sup>, lateral septal nucleus (LS)<sup>12</sup>, and paraventricular hypothalamus (PVH)<sup>13</sup>. Notably, the PVH receives sensory input from the thalamus, which modulates pain-induced fear and aversion<sup>14</sup>. Additionally, the PVH projects to the cortex and thalamus, playing an important role in processing pain information<sup>13,15</sup>. Together, these features suggest that the PVH is an important brain region for the regulation of pain and other pain-induced disorders. Activation of PVH neuron-projecting fibers in the ACC reduces presynaptic long-term potentiation (pre-LTP)<sup>16</sup>, indicating the presence of a pathway between the PVH and ACC. However, whether this pathway could be targeted to treat pain remains unclear. Moreover, both the PVH and ACC have known associations with food intake, with cholecystokinin (CCK) neurons and glutamatergic (Glu) neurons in these regions playing key roles<sup>17,18</sup>. However, the role of the pathway from CCK neurons in the paraventricular hypothalamus (PVH<sup>CCK</sup>) to glutamatergic neurons in the anterior cingulate cortex (ACC<sup>Glu</sup>) in chronic visceral pain-related changes in food preferences remains unknown. CCK is widely distributed in the gastrointestinal tract and CNS and regulates a range of physiological functions by activating its receptors<sup>13</sup>. In the CNS, CCK and its receptors contribute to the regulation of satiety, anxiety, analgesia, and dopamine-mediated behavior<sup>19</sup>. There is substantial evidence about the mechanism of action of CCK. However, relatively little is known about the role of the CCK receptor subtypes in the brain in mediating food intake.

Therefore, the aimed of this study was to determine whether a specific neural circuit exists between PVH<sup>CCK</sup> and ACC<sup>Glu</sup> neurons and whether this circuit contributes to the changes in food preference caused by chronic visceral pain in a mouse model of NCI.

We identified a circuit in which PVH<sup>CCK</sup> neurons project to ACC<sup>Glu</sup> neurons in mice. The PVH<sup>CCK</sup>-ACC<sup>Glu</sup> circuit is required for the food preference that chronic visceral pain. These results provide a theoretical basis for pain-related treatments.

## Results

### Chronic visceral pain led to changes in food preference

To explore the effects of chronic visceral pain on food preference in mice, we verified that our mouse model of chronic visceral pain induced food preference changes. Chronic visceral pain was induced by NCI, and the successful establishment of the model was verified by measuring the colorectal distention (CRD) threshold at age 6–12 weeks<sup>8</sup>. The CRD threshold was significantly lower in NCI mice than in age-matched control (CON) mice at 6–12 weeks (Fig. 1a, b,  $^{**}p < 0.01$ ,  $^{***}p < 0.001$ , two-way repeated measure ANOVA,  $n = 8$  mice), which is consistent with previous finding<sup>6</sup>. To investigate whether chronic visceral pain leads to changes in food preference in the model mice, we examined the consumption of three liquids (i.e., sucrose, water, and an intralipid solution<sup>20</sup>) and time spent in the corresponding zones in the CON and NCI mice (Fig. 1c). In the free-feeding tests, the CON mice spent more time in the intralipid zone than did the NCI mice did, whereas the NCI mice spent more time in the sucrose zone than did the CON mice did; however, there was no significant difference between groups in the time spent in the water zone (Fig. 1d).

With respect to actual food intake, the percentage of intralipid intake and time spent in the intralipid zone were significantly greater in CON mice than in NCI mice, whereas the percentage of sucrose intake and time spent in the sucrose zone were significantly lower in CON mice than in NCI mice; there was no significant difference between the groups in water intake at 12 h (Fig. 1e,  $^{**}p < 0.01$ ,  $^{***}p < 0.001$ , two-way repeated measure ANOVA,  $n = 9$  mice). Further analysis showed a positive correlation between the food intake percentage and time spent in the food zone (Fig. 1f).

NCI mice weighed significantly less than CON mice (Fig. 1g,  $^{***}p < 0.001$ , two-way repeated measure ANOVA,  $n = 8$  mice). NCI-induced chronic visceral pain was alleviated by the intraperitoneal administration of conventional analgesic agents such as ibuprofen and indomethacin (Fig. 1h,  $^{***}p < 0.001$ , two-way repeated measure ANOVA,  $n = 9$  mice), and intralipid intake was increased after drug administration compared with that before treatment in NCI mice (Fig. 1i,  $^{*}p < 0.05$ ,  $^{**}p < 0.01$ ,  $^{***}p < 0.001$ , two-way repeated measure ANOVA,  $n = 9$  mice). Together, these data suggest that chronic visceral pain leads to changes in food preference in mice.

### PVH<sup>CCK</sup> encodes chronic visceral pain-induced changes in food preference

Next, to investigate whether the PVH is involved in NCI-induced chronic visceral hypersensitivity, we compared the expression of c-Fos, an immediate early gene product and marker of neural activity<sup>21</sup>, in the PVH of mice. The number of c-Fos-expressing cells markedly increased after repetitive CRD stimulation<sup>8</sup> in NCI mice (Fig. 2a,  $^{***}p < 0.001$ , two-sided student's t-test,  $n = 6$  mice). To determine the neuronal type of the CRD-activated PVH neurons, double immunofluorescence of c-Fos with the neuron marker CCK was performed, and most c-Fos-positive neurons were colabeled with the CCK antibody (Fig. 2b).

To characterize the functional involvement of PVH<sup>CCK</sup> neurons in visceral pain perception, changes in *in vivo* Ca<sup>2+</sup> signaling were recorded using fiber photometry. AAV2/9-CCK-GCaMP6f-EGFP was injected into the PVH to label CCK neurons in NCI and CON mice (Fig. 2c). The results showed that Ca<sup>2+</sup> activity in NCI mice stimulated with the same degree of CRD was significantly higher than that in CON mice (Fig. 2d, e,  $^{**}p < 0.01$ , two-sided student's t-test,  $n = 7$  mice).

We then used patch-clamp techniques to compare the excitability of CCK neurons between NCI mice and CON mice. AAV2/9-CCK-EGFP was injected into the PVH to mark CCK neurons in NCI and CON mice (Fig. S3a). Representative images and percentage statistics showing 95% EGFP<sup>+</sup> (green) and CCK neurons (red) were colocalized in the PVH (Fig. S1a–c). When stimulated by the same current, the firing frequency of CCK neurons was significantly greater in NCI mice than in CON mice (Fig. S3b,  $^{*}p < 0.05$ ,  $^{**}p < 0.01$ , two-way repeated measure ANOVA,  $N = 9$  cells). The action potential half-width and action potential frequency of CCK neurons were significantly greater in NCI mice than in CON mice (Fig. S3c,  $^{*}p < 0.05$ ,  $^{**}p < 0.01$ , two-way repeated measure ANOVA,  $N = 9$  cells); the first spike latency and interspike interval of CCK neurons were significantly lower in NCI mice than in CON mice (Fig. S3d,  $^{*}p < 0.05$ ,  $^{**}p < 0.01$ , two-sided student's t-test,  $N = 9$  cells). Next, we used AAV2/9-CCK-hM3Dq-mCherry and AAV2/9-CCK-hM4Di-mCherry to manipulate CCK neurons in the PVH of CON mice and NCI mice, respectively (Fig. 2f). Behavioral results show that chemogenetic activation of CCK neurons by significantly decreased the CRD threshold in CON mice (Fig. 2h,  $^{***}p < 0.001$ , ordinary one-way ANOVA,  $n = 9$  mice). The percentages of intralipid intake and time spent in the intralipid zone were significantly greater in hM3Dq+normal saline (NS) mice than in hM3Dq+clozapine-N-oxide (CNO, 2.5 mg/kg, intraperitoneal) mice, whereas the percentages of sucrose intake and time spent in the sucrose zone were significantly lower in hM3Dq+NS mice than in hM3Dq+CNO mice (Fig. 2g, i,  $^{**}p < 0.01$ ,  $^{***}p < 0.001$ , two-way repeated measure ANOVA,  $n = 9$  mice). The percentage of food intake and percentage of food zone time were positively correlated (Fig. 2j).

Chemogenetic inhibition of CCK neurons significantly increased the CRD threshold in NCI mice (Fig. 2k,  $^{***}p < 0.001$ , ordinary one-way ANOVA,  $n = 9$  mice). Compared with hM4Di+CNO mice, hM4Di+NS mice showed a significantly greater percentage of sucrose intake and time spent in the sucrose zone. However, compared with hM4Di+CNO mice, hM4Di+NS mice showed significantly lower percentage of intralipid intake and spent less time in the intralipid zone (Fig. 2g, l,

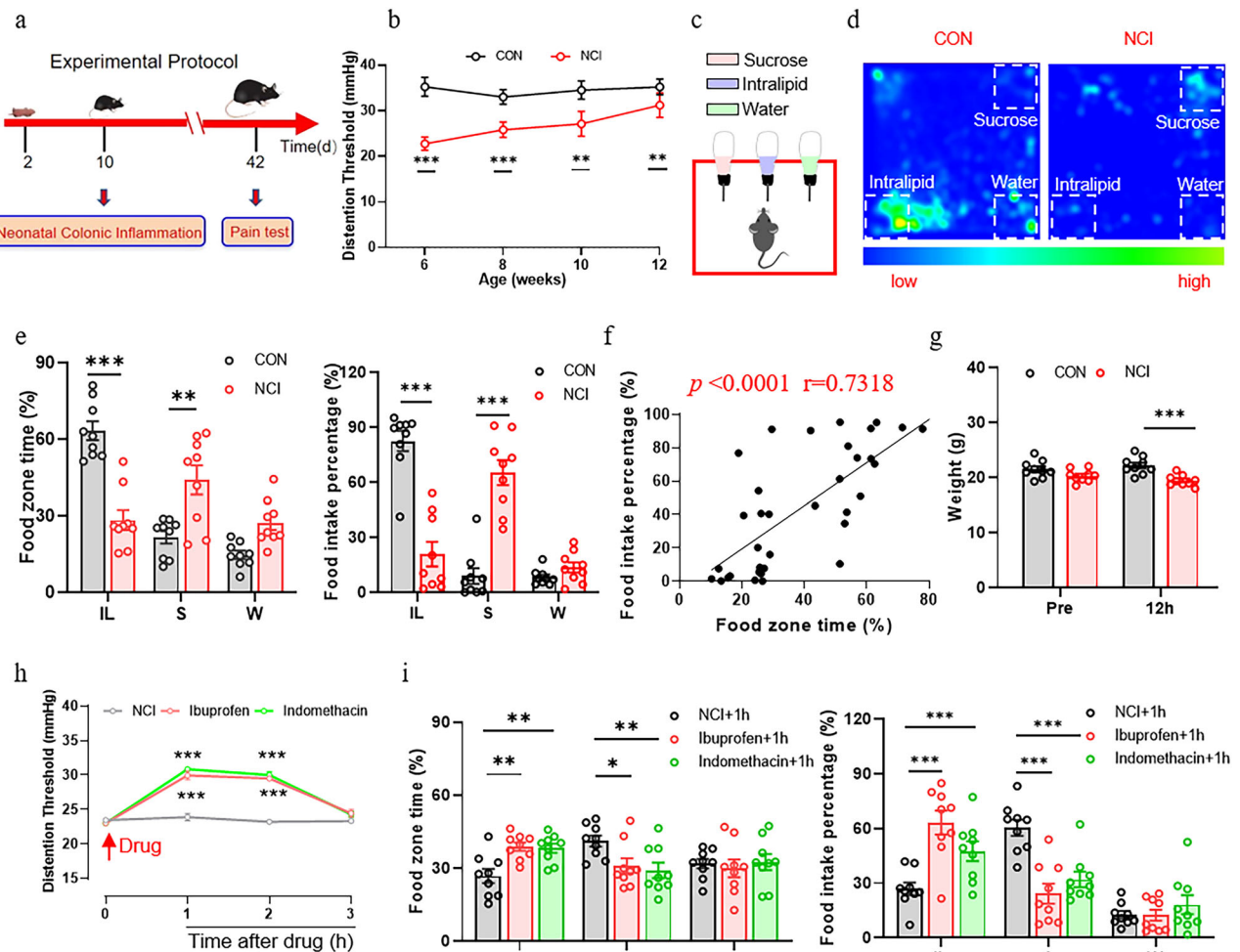


**Fig. 1 | Chronic visceral pain led to changes in food preference.** **a** Timeline for establishing and testing the chronic visceral pain model. **b** The colorectal distension (CRD) threshold in CON and NCI mice from weeks 6 to 12 ( $n = 8$  mice/group,  $p < 0.0001$  in 6 and 8 weeks,  $p < 0.0001$  in 10 weeks,  $p = 0.0011$  in 12 weeks). **c** Experimental model of food preference. **d** Heatmaps of mouse location throughout the free-feeding tests. **e** The percentage of time spent in each food zone and percentage of each type of liquid intake ( $n = 9$  mice/group, Food zone time:  $p < 0.0001$  in IL,  $p = 0.0002$  in S; Food intake percentage:  $p < 0.0001$  in IL,  $p < 0.0001$  in S). **f** Correlation between the percentage of food zone time and percentage of food intake ( $p < 0.0001$ ,  $r = 0.7318$ ). **g** Body weights of CON and NCI

mice ( $n = 9$  mice/group,  $p = 0.0003$  in 12 h). **h** Intraperitoneal injection of ibuprofen or indomethacin significantly relieved visceral pain ( $n = 9$  mice/group,  $p < 0.0001$  in ibuprofen and indomethacin). **i** The percentage of time spent in each food zone and percentage of each type of liquid intake ( $n = 9$  mice/group, Food zone time:  $p = 0.0052$  and  $0.0203$  in ibuprofen,  $p = 0.0087$  and  $0.0053$  in indomethacin; Food intake percentage:  $p < 0.0001$  in ibuprofen,  $p < 0.0001$  in indomethacin). All the data are presented as the means  $\pm$  SEMs. Two-way ANOVA with Sidak's multiple comparisons test (**b**, **e**, **g–i**). Linear regression and Correlation (**f**). \* $p < 0.05$ ; \*\* $p < 0.01$ ; \*\*\* $p < 0.001$ .

\* $p < 0.05$ , \*\* $p < 0.01$ , \*\*\* $p < 0.001$ , two-way repeated measure ANOVA,  $n = 9$  mice). The percentage of food intake and time spent in the food zone were positively correlated (Fig. 2m). Collectively, these data indicate that PVH<sup>CK</sup> neurons are involved in the modulation of chronic visceral pain-induced food preference changes in mice.

### PVH<sup>CK</sup> neurons projected to ACC<sup>Glu</sup> neurons

To identify the neural circuits involving PVH<sup>CK</sup> neurons in chronic visceral pain, we identified the regions downstream of the PVH that respond to visceral pain. The anterograde tracer AAV2/9-hSyn-EGFP was injected into the PVH. EGFP<sup>+</sup> fibers were observed in the ACC at 3 weeks post-injection (Fig. 3a). In addition, EGFP<sup>+</sup> fibers were observed in other brain regions, such as the lateral septal (LS), paraventricular thalamic nucleus (PVT), claustrum (CL) and insular cortex (IC) (Fig. S2a, b). To further explore the connection of PVH with ACC and the monosynaptic rabies-based retrograde tracing was performed in VGlut2-Cre mice. Cre-dependent helper viruses (a mixture of AAV-EF1a-DIO-TVA-GFP and AAV-EF1a-DIO-RVG) were injected into the ACC,

while an EnvA-pseudotyped RV-ΔG-DsRed rabies virus (RV) was injected into the same site in VGlut2-Cre mice 3 weeks later, revealing DsRed-positive neurons in the PVH (Fig. 3b). The results shown that glutamatergic neurons of ACC connection with PVH. To verify the PVH-ACC pathway, the retrograde tracer virus AAV2/R-hSyn-EGFP was injected into the ACC. GFP-labeled signals were observed not only in the ACC but also in the prefrontal cortex, claustrum, insular cortex, and PVH (Fig. 3c, d).

We then investigated whether ACC<sup>Glu</sup> receives direct projections from PVH<sup>CK</sup>. AAV2/9-EF1a-Dio-hM4Di/hM3Dq-mCherry and AAV2/9-CCK-Cre were injected into the PVH to mark CCK neurons, whereas AAV2/9-VGlut2-GCaMP6f-EGFP was injected into the ACC to mark Glu neurons in NCI and CON mice, and the representative image of virus in the PVH and ACC (Fig. 3e). The data indicated that Ca<sup>2+</sup> inhibition in hM4Di+CNO mice was significantly lower with the same CRD than that in hM4Di+NS mice (Fig. 3f, g, \* $p < 0.05$ , two-sided student's t-test,  $n = 7$  mice). The Ca<sup>2+</sup> activity in hM3Dq+CNO mice stimulated with the same degree of CRD was significantly greater than that in hM3Dq+NS mice



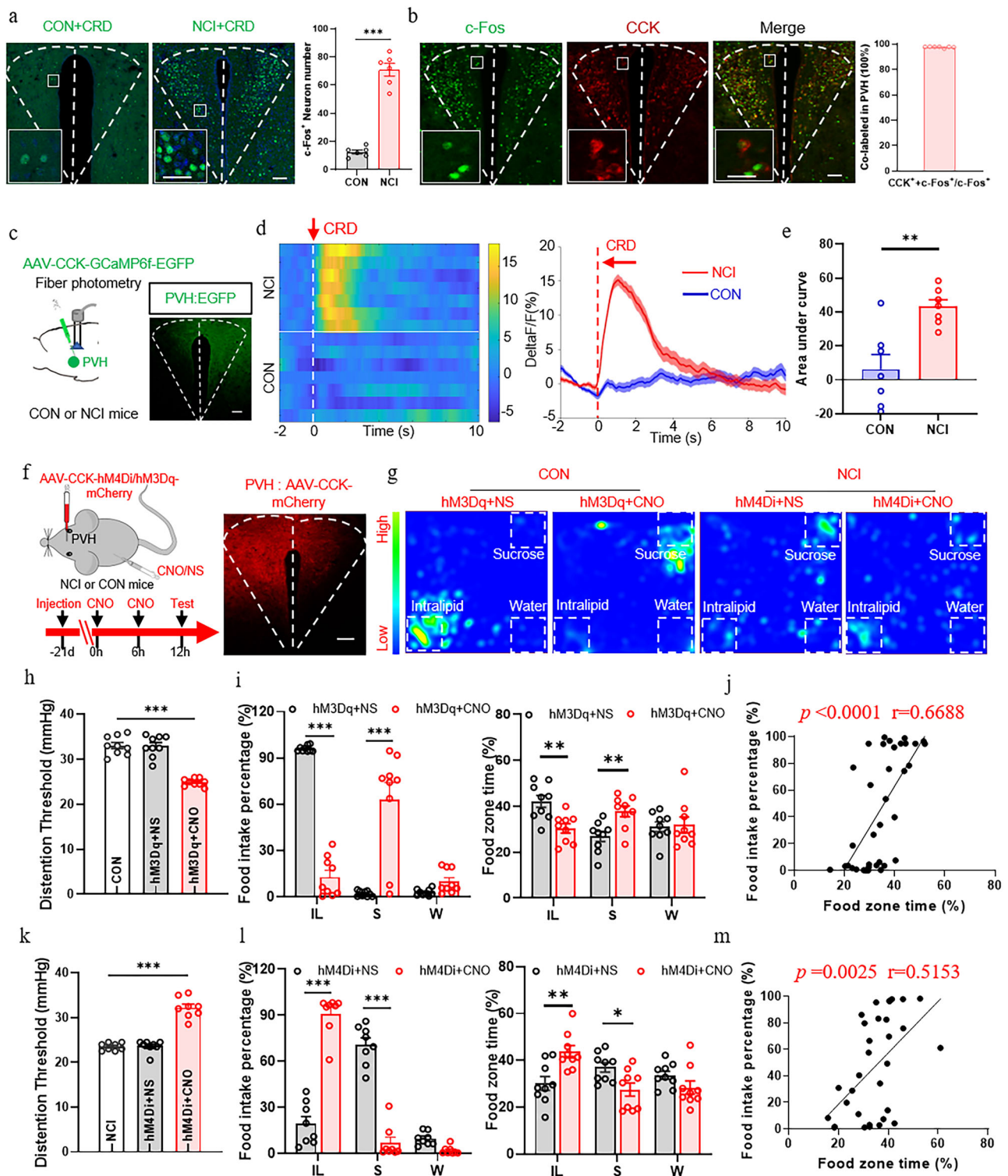


(Fig. 3h, i,  $*p < 0.05$ , two-sided student's t-test,  $n = 7$  mice). These findings suggest that CCK-positive neurons in the PVH may play a regulatory role in the modulation of ACC<sup>Glu</sup>.

### ACC<sup>Glu</sup> modulates chronic visceral pain-induced changes in food preference

Next, to investigate whether the ACC is involved in NCI-induced chronic visceral hypersensitivity, we compared the ACC expression of c-Fos in the NCI and CON mice. The number of c-Fos-expressing cells was markedly increased following repeated CRD stimulation<sup>8</sup> in NCI

mice (Fig. 4a,  $***p < 0.001$ , two-sided student's t-test,  $n = 6$  mice). To explore the specific neurons within the ACC that are involved in visceral pain, activated c-Fos neurons were double-labeled with a glutamate antibody to mark forebrain excitatory neurons; the majority of the c-Fos<sup>+</sup> neurons were colabeled with the glutamate antibody (Fig. 4b). To further characterize the Glu neurons activated in the ACC after visceral stimulation, fiber photometry was used to record changes in Ca<sup>2+</sup> signaling in vivo before and after stimulation. Specifically, AAV2/9-VGlu2-GCaMP6f-EGFP was injected into the ACC to label the Glu neurons in NCI and CON mice (Fig. 4c). The Ca<sup>2+</sup> activity in NCI

**Fig. 2 | PVH<sup>CCK</sup> encodes chronic visceral pain-induced change in food preference.** **a** Representative images of c-Fos expression after CRD stimulation and the total number of c-Fos-expressing neurons ( $n = 3$  mice,  $p < 0.0001$ ). Scale bar: 20  $\mu\text{m}$ . **b** Representative images of coexpressing c-Fos (green) and CCK (red) neurons and the percentage of coexpressing c-Fos in the PVH ( $n = 3$  mice). Scale bar: 20  $\mu\text{m}$ . **c** Schematic of the optical fiber photometry assay and representative images of EGFP expression in the PVH. Scale bar: 20  $\mu\text{m}$ . **d** Heatmaps and average calcium activity showing  $\text{Ca}^{2+}$  signals time-locked to the CRD stimulus in NCI and CON mice. **e** Area under the curve of  $\text{Ca}^{2+}$  activity in PVH CCK-positive neurons from NCI and CON mice receiving CRD stimulation ( $n = 7$  mice,  $p = 0.0022$ ). **f** Schematic of viral injection (top) and the experimental protocol of chemogenetics (bottom) and representative images of mCherry expression in the PVH. Scale bar: 20  $\mu\text{m}$ . **g** Heatmaps of mouse location during the free-feeding tests. **h** Colorectal distention (CRD) threshold changes before and after hM3Dq activation of PVH<sup>CCK</sup> neurons in

CON mice ( $n = 9$  mice/group,  $p < 0.0001$ ). **i** Percentage of time and intake for each type of food before and after hM3Dq activation of PVH<sup>CCK</sup> neurons in CON mice ( $n = 9$  mice/group, Food intake percentage:  $p < 0.0001$ ; Food zone time:  $p = 0.0049$  in IL and  $p = 0.0097$  in S). **j** Correlation between the percentage of food zone time and percentage of food intake ( $p < 0.0001$ ,  $r = 0.6688$ ). **k** CRD threshold before and after hM4Di inhibition of PVH<sup>CCK</sup> neurons in NCI mice ( $n = 9$  mice/group,  $p < 0.0001$ ). **l** The percentage of food zone time and intake for each food type before and after hM4Di inhibition of PVH<sup>CCK</sup> neurons in NCI mice ( $n = 9$  mice/group, Food intake percentage:  $p < 0.0001$ ; Food zone time:  $p = 0.0013$  in IL and  $p = 0.032$  in S). **m** Correlation between the percentage of food zone time and percentage of food intake ( $p = 0.0025$ ,  $r = 0.5153$ ). All the data are presented as the means  $\pm$  SEMs. Two-sided student's *t* test (**a**, **e**). Two-way ANOVA with Sidak's multiple comparisons test (**i**, **l**). Ordinary one-way ANOVA with Dunnett's multiple comparisons test (**h**, **k**). Linear regression and Correlation (**j**, **m**).  $^*p < 0.05$ ;  $^{**}p < 0.01$ ;  $^{***}p < 0.001$ .

mice was significantly greater than that in CON mice was stimulated with the same degree of CRD (Fig. 4d, e,  $^*p < 0.05$ , two-sided student's *t*-test,  $n = 7$  mice).

Simultaneously, patch-clamp techniques were employed to compare the excitability of Glu neurons in NCI and CON mice. AAV2/9-VGlut2-EGFP was injected into the ACC to label Glu neurons in NCI and CON mice (Fig. S4a). When stimulated by the same current, the firing frequency of Glu neurons was significantly greater in NCI mice than in CON mice (Fig. S4b,  $^{***}p < 0.001$ , two-way repeated measure ANOVA,  $N = 7$  cells). The action potential half-width and action potential frequency of Glu neurons were significantly greater in NCI mice than in CON mice (Fig. S4c,  $^*p < 0.05$ ,  $^{***}p < 0.001$ , two-way repeated measure ANOVA,  $N = 7$  cells); the first spike latency and interspike interval of Glu neurons were significantly lower in NCI mice than in CON mice (Fig. S4d,  $^*p < 0.05$ , two-sided student's *t*-test,  $N = 7$  cells). Next, AAV2/9-VGlut2-hM3Dq-mCherry and AAV2/9-VGlut2-hM4Di-mCherry were used to label the Glu neurons in the ACC of CON and NCI mice, respectively (Fig. 4f). The results demonstrated that the chemogenetic activation of Glu neurons significantly decreased the CRD threshold (Fig. 4h,  $^{***}p < 0.001$ , ordinary one-way ANOVA,  $n = 9$  mice). The percentage of intralipid intake and time spent in the intralipid zone were significantly greater in hM3Dq+NS mice than in hM3Dq+CNO mice, whereas the percentage of sucrose intake and time spent in the sucrose zone were significantly lower (Fig. 4g, i,  $^*p < 0.05$ ,  $^{**}p < 0.01$ , two-way repeated measure ANOVA,  $n = 9$  mice). The percentage of food intake and the time spent in the food zone were positively correlated (Fig. 4j).

Chemogenetic inhibition of Glu neurons significantly increased the CRD threshold (Fig. 4k,  $^{***}p < 0.001$ , ordinary one-way ANOVA,  $n = 9$  mice). The percentage of sucrose intake and the percentage of time spent in the sucrose zone were significantly greater in hM4Di+NS mice than in hM4Di+CNO mice, whereas the percentage of intralipid intake and the percentage of time spent in the intralipid were significantly lower (Fig. 4g, l,  $^*p < 0.05$ ,  $^{**}p < 0.01$ , two-way repeated measure ANOVA,  $n = 9$  mice). The percentage of food intake and the time spent in the food zone were positively correlated (Fig. 4m). These data indicate that ACC<sup>Glu</sup> is involved in the changes in food preference induced by chronic visceral pain in mice.

### The PVH<sup>CCK</sup>-ACC<sup>Glu</sup> circuit regulates chronic visceral pain-induced changes in food preference

To explore CCK neuron signaling from the PVH to the ACC, we performed chemogenetic manipulation of the PVH<sup>CCK</sup>-ACC<sup>Glu</sup> projections with a designer drug approach that exclusively activates certain receptors. AAV2/9-EF1a-Dio-hM3Dq-mCherry and AAV2/9-CCK-Cre were injected into the PVH of CON and NCI mice, and AAV2/9-EF1a-Dio-hM4Di-mCherry and AAV2/9-CCK-Cre were injected into the PVH of NCI mice, and the representative image of virus in the PVH (Fig. 5a). Patch-clamp recordings on the ACC brain slices showed that, CNO (5  $\mu\text{M}$ )<sup>22</sup> treatment significantly increased the amplitude and frequency

(Fig. 5b, S5a,  $^*p < 0.05$ , two-sided student's *t*-test,  $N = 7$  cells) of spontaneous excitatory postsynaptic currents (sEPSCs) in ACC neurons from CON mice with PVH infection of hM3Dq. Conversely, CNO (5  $\mu\text{M}$ ) treatment significantly decreased the amplitude and frequency (Fig. 5b, S5b,  $^*p < 0.05$ , two-sided student's *t*-test,  $N = 7$  cells) of sEPSCs in ACC neurons from NCI mice with PVH infection of hM4Di.

Next, we determined whether the PVH<sup>CCK</sup>-ACC<sup>Glu</sup> neural circuit regulated the changes in mouse food preferences associated with chronic visceral pain. AAV2/9-EF1a-Dio-hM3Dq-mCherry and AAV2/9-CCK-Cre were injected into the PVH of CON mice, and AAV2/9-EF1a-Dio-hM4Di-mCherry and AAV2/9-CCK-Cre were injected into the PVH of NCI mice. Cannulas were bilaterally implanted into the ACC of the mice 2 weeks after virus injection. CNO was delivered via cannulas to activate or inactivate the PVH<sup>CCK</sup> terminals in the ACC (Fig. 5c). The chemogenetic activation of CCK neuron terminals significantly decreased the CRD threshold (Fig. 5e,  $^{***}p < 0.001$ , ordinary one-way ANOVA,  $n = 9$  mice). The percentage of intralipid intake and the percentage of time spent in the intralipid zone were significantly increased in hM3Dq+NS mice compared with hM3Dq+CNO mice. Meanwhile, the percentage of sucrose intake and time spent in the sucrose zone were significantly lower than that consumed by the hM3Dq+CNO mice (Fig. 5d, f,  $^*p < 0.05$ ,  $^{**}p < 0.01$ ,  $^{***}p < 0.001$ , two-way repeated measure ANOVA,  $n = 9$  mice). The food intake percentage and food zone percentage were positively correlated (Fig. 5g).

Chemogenetic inhibition of CCK neuron terminals significantly increased the CRD threshold (Fig. 5h,  $^{***}p < 0.001$ , ordinary one-way ANOVA,  $n = 9$  mice). The percentage of sucrose intake and the percentage of time spent in the sucrose zone were significantly greater in the hM4Di+NS mice than in the hM4Di+CNO mice. In contrast, the percentages of intralipid intake and time spent in the intralipid zone in hM4Di+CNO mice were significantly lower than those in hM4Di+CNO mice (Fig. 5d, i,  $^{**}p < 0.01$ , two-way repeated measure ANOVA,  $n = 9$  mice). The percentage of food intake and percentage of food zone time were positively correlated (Fig. 5j). These data indicate that the projections from PVH<sup>CCK</sup> to ACC<sup>Glu</sup> neurons play a role in chronic visceral pain-induced changes in food preference.

### ACC expression of CCKB receptors is increased in NCI mice

Chronic visceral pain was induced through NCI in 6–12 weeks<sup>6</sup>. ACC expression of CCK receptors was then assessed 9 weeks after NCI induction. CCKB receptors (CCKBRs) expression at both the protein and mRNA levels was significantly greater in the bilateral ACC of NCI mice than that in CON mice. However, the protein and mRNA levels of CCKA receptors (CCKARs) were not significantly upregulated in the ACC of either hemisphere (Fig. 6a–c,  $^{**}p < 0.01$ , two-way repeated measure ANOVA,  $n = 6$  mice). Subsequently, we microinjected a CCKBRs agonist (tetragastrin [Tet], 30  $\mu\text{M}$ , MCE, Shanghai, China) or antagonist (proglumide sodium [Pro], 30  $\mu\text{M}$ , MCE)<sup>23</sup> into the right ACC region with a cannula to examine there effects in NCI and CON mice (Fig. 6d). Tetragastrin significantly decreased the CRD threshold

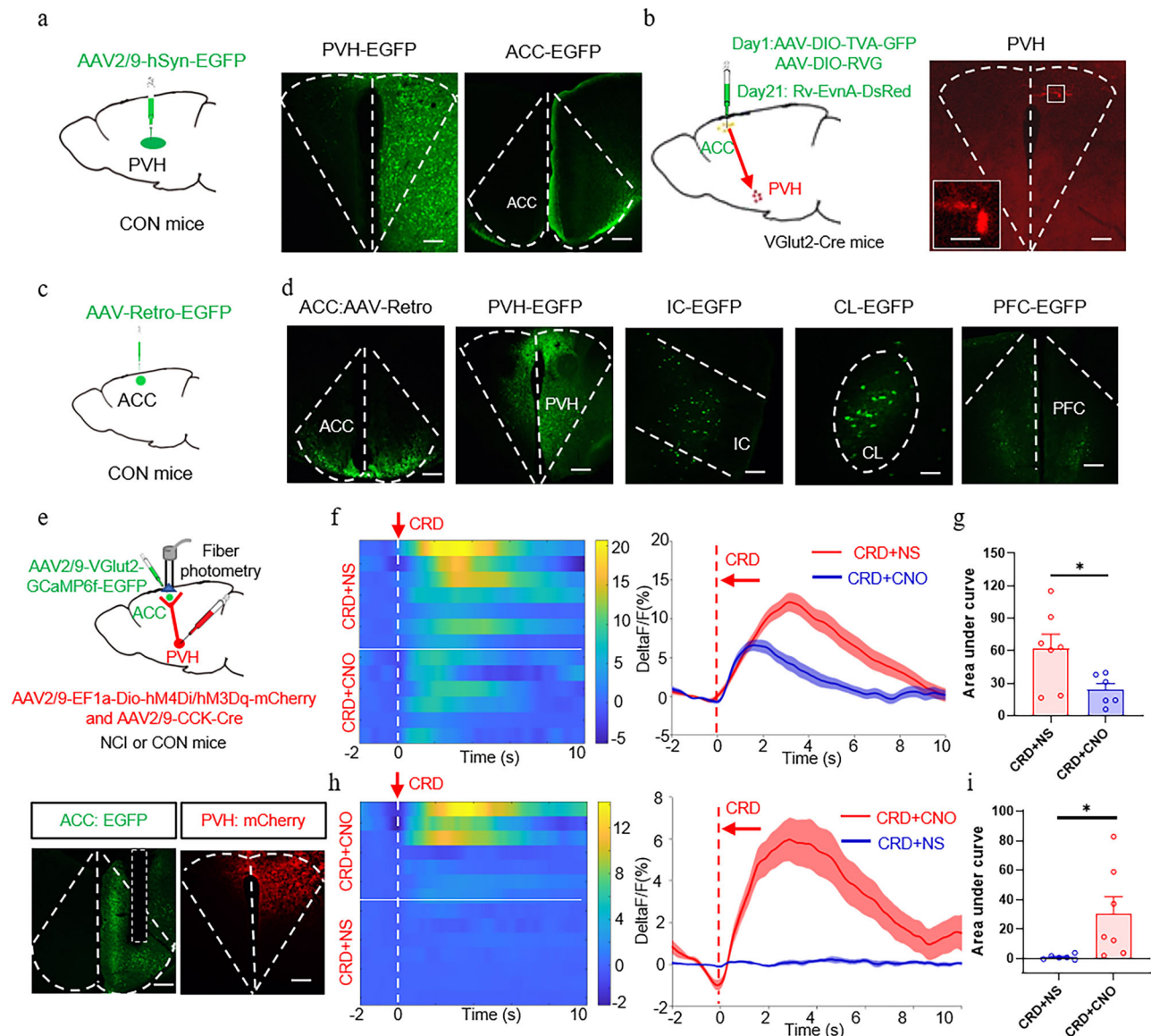


**Fig. 3 | PVH<sup>CCK</sup> neurons projected to ACC<sup>Glu</sup> neurons.** **a** Schematic of the anterograde virus tracing strategy (left) and typical images of virus injection sites within the PVH and viral expression in the ACC (right). Scale bar: 20  $\mu$ m. **b** Schematic of virus injection (left) and representative images showing RV-DsRed expression in the PVH (right). Scale bar: 20  $\mu$ m. **c** Schematic of the retrograde virus tracing strategy. **d** Typical images of virus injection sites within the ACC and viral expression in other brain regions. Scale bar: 20  $\mu$ m. **e** Schematic of viral injection and the real-time optical fiber photometry assay (top) and representative images showing EGFP and mCherry expression in the ACC and PVH (bottom). Scale bar: 20  $\mu$ m. **f** Heatmaps and

average Ca<sup>2+</sup> transient signals of ACC<sup>Glu</sup> neurons in hM4Di+CNO and hM4Di+NS mice receiving CRD stimulation. **g** Area under the curve of Ca<sup>2+</sup> activity of ACC<sup>Glu</sup> neurons in hM4Di+CNO and hM4Di+NS mice receiving CRD stimulation ( $n = 7$  mice/group,  $p = 0.0337$ ). **h** Heatmaps and average Ca<sup>2+</sup> transient signals of ACC<sup>Glu</sup> neurons in hM3Dq+CNO and hM3Dq+NS mice receiving CRD stimulation. **i** Area under the curve of Ca<sup>2+</sup> activity of ACC<sup>Glu</sup> neurons in hM3Dq+CNO and hM3Dq+NS mice receiving CRD stimulation ( $n = 7$  mice/group,  $p = 0.0413$ ). All the data are presented as the means  $\pm$  SEMs. Two-sided student's *t* test (**g**, **i**). \* $p < 0.05$ .

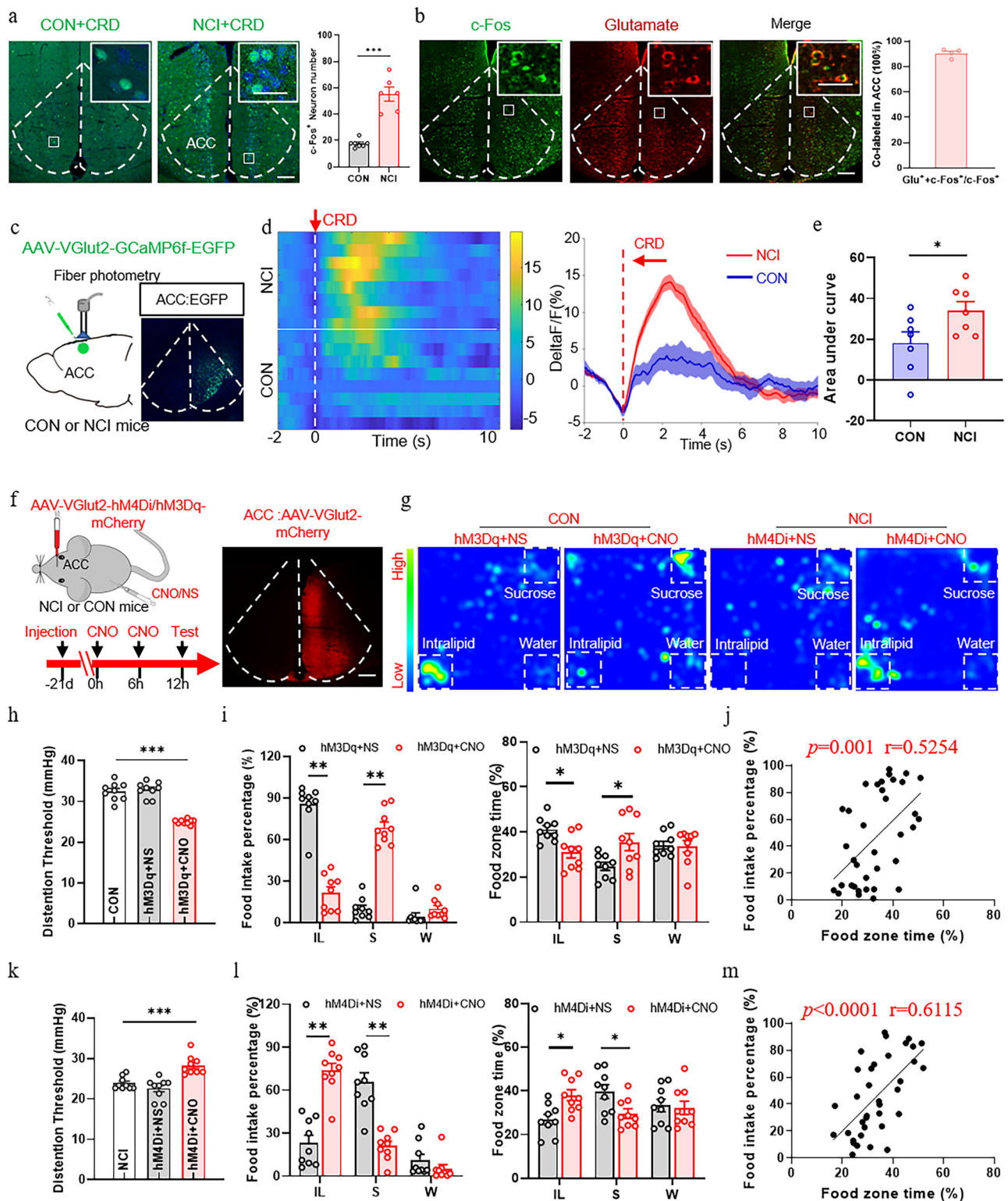
in CON mice, whereas proglumide sodium significantly increased the CRD threshold in NCI mice. (Fig. 6e, f, \*\* $p < 0.01$ , ordinary one-way ANOVA,  $n = 8$  mice). Next, the location of the CCKBRs in the ACC was verified by immunofluorescence. CCKBRs exhibited considerable colocalization with Glu neurons, with a colocalization ratio of 89.4% (Fig. 6g, h). These findings suggest that the overactivity of CCKBRs in the ACC region may contribute to the central sensitization of NCI mice to chronic visceral pain.

### CCKBRs mediate the regulatory role of the PVH<sup>CCK</sup>-ACC<sup>Glu</sup> circuit in chronic visceral pain-induced food preference changes

Finally, we investigated the molecular mechanisms through which CCKBRs are involved in chronic visceral pain in NCI mice. Specifically,

proglumide sodium was used to modulate the sEPSCs of glutamatergic neurons in ACC slices from NCI mice. AAV2/9-CCK-hM3Dq-mCherry and AAV2/9-VGlut2-EGFP were used to label CCK neurons and glutamatergic neurons, respectively, in CON mice (Fig. 7a). The typical current traces (Fig. 7b), and histogram results demonstrated that CNO activation of the PVH<sup>CCK</sup> terminals in the ACC significantly enhanced the frequency and amplitude of sEPSCs in ACC<sup>Glu</sup>. This effect was reversed by proglumide sodium inhibition of CCKBRs in the ACC (Fig. 7c, and S6a, \* $p < 0.05$ , ordinary one-way ANOVA,  $N = 8$  cells). Meanwhile, AAV2/9-CCK-hM4Di-mCherry and AAV2/9-VGlut2-EGFP were used to label CCK neurons and glutamatergic neurons, respectively, in NCI mice (Fig. 7d). As shown in Fig. 7e, the typical current traces, and histogram results supported that CNO activation of PVH<sup>CCK</sup>





terminals in the ACC significantly reduced the frequency and amplitude of sEPSCs in ACC<sup>Glu</sup>. This effect was reversed by tetragastrin-induced activation of CCKBRs in the ACC (Fig. 7f, S6b, \* $p$  < 0.05, ordinary one-way ANOVA,  $N$  = 6 cells). Next, we explored whether CCKBRs were involved in the PVH to ACC circuit. At 3 weeks following the injection of AAV2/9-EF1a-Dio-hM3Dq-mCherry and AAV2/9-CCK-Cre into the PVH of CON mice (Fig. 7g), CNO-induced activation of PVH<sup>CCK</sup> terminals in the ACC significantly decreased the CRD threshold, as well as the percentage of intralipid intake and time spent in the

intralipid zone. This effect was reversed by proglumide sodium inhibition of CCKBRs in the ACC (Fig. 7h-j, \* $p$  < 0.05, \*\* $p$  < 0.01, \*\*\* $p$  < 0.001, ordinary one-way ANOVA and two-way repeated measure ANOVA,  $n$  = 8 mice). The food intake percentage and food zone time percentage were positively correlated (Fig. 7k).

Conversely, 3 weeks after AAV2/9-EF1a-Dio-hM4Di-mCherry and AAV2/9-CCK-Cre were injected into the PVH of NCI mice (Fig. 7g), CNO inhibition of PVH<sup>CCK</sup> terminals in the ACC significantly enhanced the CRD threshold and increased the percentage of intralipid intake and

**Fig. 4 | ACC<sup>Glu</sup> modulates chronic visceral pain-induced change in food preference.** **a** Representative images of c-Fos expression following CRD stimulation in the ACC and the total number of c-Fos-expressing neurons ( $n = 3$  mice,  $p < 0.0001$ ). Scale bar: 20  $\mu\text{m}$ . **b** Representative images showing the coexpression of c-Fos neurons (green) and glutamatergic neurons (red) in the ACC, along with the percentage of coexpressed neurons ( $n = 3$  mice). Scale bar: 20  $\mu\text{m}$ . **c** Schematic representation of the optical fiber photometry assay and representative images of EGFP expression in the ACC. Scale bar: 20  $\mu\text{m}$ . **d** Heatmaps and average calcium activity showing  $\text{Ca}^{2+}$  signals time-locked to the CRD stimuli in NCI and CON mice. **e** Area under the curve of  $\text{Ca}^{2+}$  activity in Glu-positive ACC neurons in CON and NCI mice receiving CRD stimulation ( $n = 7$  mice,  $p = 0.0435$ ). **f** Schematic of viral injection (top) and experimental protocol of chemogenetic (bottom) and representative images of mCherry expression in the ACC. Scale bar: 20  $\mu\text{m}$ . **g** Spatial location heatmaps from free-feeding tests. **h** Colorectal distention (CRD) thresholds before and after hM3Dq activation of ACC<sup>Glu</sup> neurons in

CON mice ( $n = 9$  mice/group,  $p < 0.0001$ ). **i** Percentage of time spent in each food zone and intake of each food type before and after hM3Dq activation of ACC<sup>Glu</sup> neurons in CON mice ( $n = 9$  mice/group, Food intake percentage:  $p < 0.0001$ , Food zone time:  $p = 0.0173$  in IL and  $p = 0.0107$  in S). **j** Correlation between the percentage of food zone time and percentage of food intake ( $p = 0.001$ ,  $r = 0.5254$ ). **k** CRD threshold before and after hM4Di inhibition of ACC<sup>Glu</sup> neurons in NCI mice ( $n = 9$  mice,  $p = 0.0005$ ). **l** The percentage of food zone time and food intake for each food before and after hM4Di inhibition of ACC<sup>Glu</sup> neurons in NCI mice ( $n = 9$  mice/group, Food intake percentage:  $p < 0.0001$ , Food zone time:  $p = 0.0172$  in IL and  $p = 0.0356$  in S). **m** Correlation between the percentage of food zone time and percentage of food intake ( $p < 0.0001$ ,  $r = 0.6115$ ). All the data are presented as the means  $\pm$  SEMs. Two-sided student's *t* test (**a**, **e**). Two-way ANOVA with Sidak's multiple comparisons test (**i**, **l**). Ordinary one-way ANOVA with Dunnett's multiple comparisons test (**h**, **k**). Linear regression and Correlation (**j**, **m**). \* $p < 0.05$ ; \*\* $p < 0.01$ ; \*\*\* $p < 0.001$ .

time spent in the intralipid zone. This effect was reversed by tetra-gastrin activation of CCKBRs in the ACC. (Fig. 7h, l, m, \* $p < 0.05$ , \*\* $p < 0.01$ , ordinary one-way ANOVA and two-way repeated measure ANOVA,  $n = 8$  mice). The food intake percentage and food zone time percentage were positively correlated (Fig. 7n). Overall, these findings indicate that CCKBRs overactivity in the ACC likely contributes to chronic visceral pain and subsequent alterations in food preference in NCI mice.

## Discussion

Chronic visceral pain is associated with discomfort and emotional changes. Fat and sugar are important nutrients, and dedicated neural circuits drive their consumption<sup>24–26</sup>. While the neural circuits that drive food intake have been studied<sup>20</sup>, how neurons in central brain regions integrate nociceptive signals to mediate food preference mechanisms in chronic visceral pain has not been assessed to date; specifically, it has been unclear whether and how the PVH projects to feeding-related brain regions to modulate feeding preferences during chronic visceral pain. Our data revealed that PVH<sup>CCK</sup> neurons were involved in the modulation of food preference in this mouse model of chronic visceral pain (Fig. 2). Further, PVH<sup>CCK</sup> neurons directly activated ACC<sup>Glu</sup> neurons to modulate food preference in NCI mice. The inhibition of PVH<sup>CCK</sup> terminals in the ACC relieved chronic visceral pain and altered feeding choices in NCI mice (Fig. 5). Our findings provide an insights into the relationship between chronic visceral pain and food preferences.

The PVH plays a role in feeding behavior<sup>27,28</sup>, along with temperature-regulated circuits for feeding behavior<sup>29</sup>. Although the PVH is involved in both chronic visceral pain<sup>30</sup> and feeding behaviors, the precise relationship between chronic visceral pain and food preference remains unclear. Our data revealed that the PVH was involved in the modulation of food preference in mice with chronic visceral pain. The PVH is located mainly in the thalamus with components on both sides of the third ventricle. It contains numerous types of neurons, each with distinct roles. For example, oxytocinergic neurons innervate sympathetic premotor neurons in the rostral medullary raphe region to stimulate brown adipose tissue thermogenesis and regulate cardiovascular functions<sup>31</sup>. Meanwhile, glutamatergic neurons are critical for both arousal and maintenance<sup>32</sup>. However, our electrophysiological results revealed significantly greater excitability of CCK neurons in NCI mice than in CON mice. In NCI mice, chemogenetic inhibition of PVH<sup>CCK</sup> neurons significantly reduced chronic visceral pain, and food preference shifted from sucrose to intralipids (Fig. 2). Chemogenetic activation of PVH<sup>CCK</sup> neurons significantly lowered the visceral pain threshold in CON mice, and the food preference shifted from intralipids to sucrose (Fig. 2). Therefore, our results suggest that CCK neurons play a significant role in modulating food preference in the context of chronic visceral pain.

Using a dual-virus strategy, we confirmed a direct neural connection between the PVH and ACC (Fig. 3), which is consistent with previous findings that the PVH region projected directly to the ACC region<sup>16,33</sup>. The ACC region plays a crucial role in the CNS and is involved in modulating pain<sup>8</sup> and social behavior impairment<sup>34,35</sup>. It contains various types of neurons, including glutamatergic<sup>36</sup>, GABAergic<sup>37</sup>, and parvalbumin neurons<sup>18</sup>. To determine the type of ACC neurons mediating the relationship between chronic visceral pain and changes in food preference, several techniques, including immunofluorescence, in vivo optical fiber recording, and chemogenetics, have been employed. One important finding was the identification of a direct PVH<sup>CCK</sup>-ACC<sup>Glu</sup> neural circuit that uniquely mediated chronic visceral pain accompanied by a change in food preference (Fig. 5).

Electrophysiological and chemogenetic results revealed that the activation of PVH<sup>CCK</sup> neuron terminals in the ACC slices significantly enhanced Glu neuron excitability and lowered the visceral pain threshold in CON mice, shifting their food preference from the intralipid solution to sucrose (Fig. 5). Inhibition of PVH CCK neurons terminals in ACC slices significantly reduced Glu neuron excitability and visceral pain in NCI mice, with their food preference shifting from sucrose solution to the intralipid solution (Fig. 5). However, additional studies are necessary to investigate the molecular mechanisms by which the PVH-ACC pathway regulates visceral pain and accompanying changes in food preference.

Although the mechanism by which ACC<sup>Glu</sup> are activated by the stimulation of presynaptic CCK neurons is the PVH is not fully understood, our data indicate that an excess of CCKBRs subunits and over-activity of the ACC<sup>Glu</sup> neurons may account for the central sensitization of the PVH<sup>CCK</sup>-ACC<sup>Glu</sup> neural circuit in NCI mice that show both chronic visceral pain and changes in food preference. CCK and its receptors are widely distributed in the CNS and contribute to the regulation of satiety, anxiety, and analgesia and dopamine-mediated behaviors<sup>19</sup>. Modern molecular biological techniques have identified two CCK receptors: CCKARs and CCKBRs<sup>38</sup>. CCKARs are involved in gastrointestinal motor function<sup>39</sup>. One study revealed that depression can be treated with CCKBRs antagonists, which blocked long-term delay in the basolateral amygdala<sup>40</sup>. Our results indicated that CCKBRs were activated in chronic visceral pain and that a CCKBRs antagonist could alleviate chronic visceral pain in NCI mice, which led to a shift in food preference from sucrose solution to intralipid solution (Fig. 7).

Previous studies have reported that pain-induced learning and memory impairments might be due to hyperexcitation of neurons in the central nervous system<sup>41</sup>. Our results showed that the neural circuit of cholecystokinin neurons in the PVH projecting to glutamatergic neurons in the ACC regulated food preference under chronic visceral pain conditions. Since the present study primarily focused on the central mechanisms by which chronic visceral pain drives changes in food preference, we did not observe whether the pain-induced



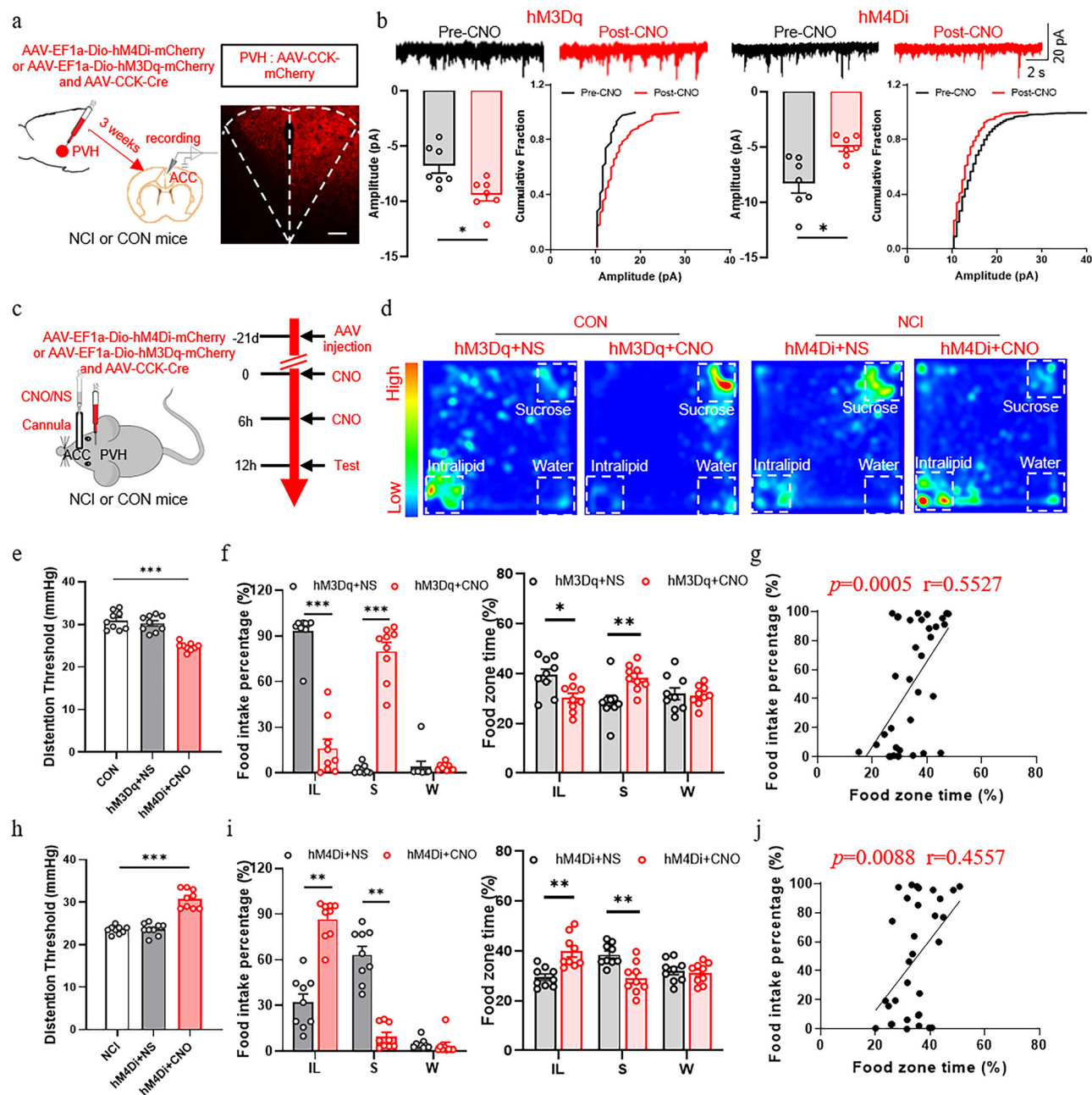


**Fig. 5 | PVH<sup>CK</sup>-ACC<sup>Glu</sup> circuit regulates chronic visceral pain-induced changes in food preference.** **a** Schematic of chemogenetics manipulation (left) and representative images of chemogenetic viral expression in the PVH (right). Scale bar: 20  $\mu$ m. **b** Top: Representative traces of sEPSCs in ACC neurons following bath application of ACSF and then CNO. Bottom: sEPSC peak amplitude and cumulative fraction plots ( $n = 7$  cells/group, Pre+hM3Dq vs Post+hM3Dq,  $p = 0.0349$ ; Pre+hM4Di vs Post+hM4Di,  $p = 0.0255$ ). **c** Schematic of chemogenetic manipulation (left) and the experimental protocol of chemogenetic manipulation (right). **d** Heatmaps of mouse location during the free-feeding tests. **e** Colorectal distension thresholds before and after hM3Dq activation of PVH<sup>CK</sup> neurons terminal in the ACC region in CON mice ( $n = 9$  mice/group,  $p < 0.0001$ ). **f** Food zone time percentage and food intake percentage for each liquid type before and after hM3Dq activation of PVH<sup>CK</sup> neurons terminal in the ACC region in CON mice ( $n = 9$  mice/group, Food intake percentage,  $p < 0.0001$ ; Food zone time, IL:hM3Dq+NS vs

hM3Dq+CNO,  $p = 0.0103$ , S: hM3Dq+NS vs hM3Dq+CNO,  $p = 0.0059$ ). **g** Correlation between the percentage of food zone time and percentage of food intake ( $p = 0.0005$ ,  $r = 0.5527$ ). **h** CRD threshold before and after hM4Di inhibition of PVH<sup>CK</sup> neurons terminal in the ACC region in NCI mice ( $n = 9$  mice/group,  $p < 0.0001$ ). **i** The percentage of food zone time and percentage of intake for each of the three liquids before and after hM4Di inhibition of the PVH<sup>CK</sup> neurons terminating in the ACC region in NCI mice ( $n = 9$  mice/group, Food intake percentage,  $p < 0.0001$ ; Food zone time:  $p = 0.0002$  in IL and  $p = 0.0007$  in S). **j** Correlation between the percentage of food zone time and percentage of food intake ( $p = 0.0088$ ,  $r = 0.4557$ ). All the data are presented as the means  $\pm$  SEMs. Two-sided student's  $t$  test (**b**). Two-way ANOVA with Sidak's multiple comparisons test (**f**, **i**). Ordinary one-way ANOVA with Dunnett's multiple comparisons test (**e**, **h**). Linear regression and Correlation (**g**, **j**). \* $p < 0.05$ ; \*\* $p < 0.01$ ; \*\*\* $p < 0.001$ .

changes in food preference might disrupt learning and memory. Since alterations in the PVH-ACC circuit may affect synaptic plasticity, we therefore speculate that it might influence learning and memory processes. The potential impact and mechanisms of chronic visceral pain

on learning and memory require further investigation. Relevant descriptions have been added in the discussion section.

The sweet compounds are pain relievers<sup>42,43</sup>, but the mechanism is unclear. A recent study showed that the gut-brain axis mediates sugar

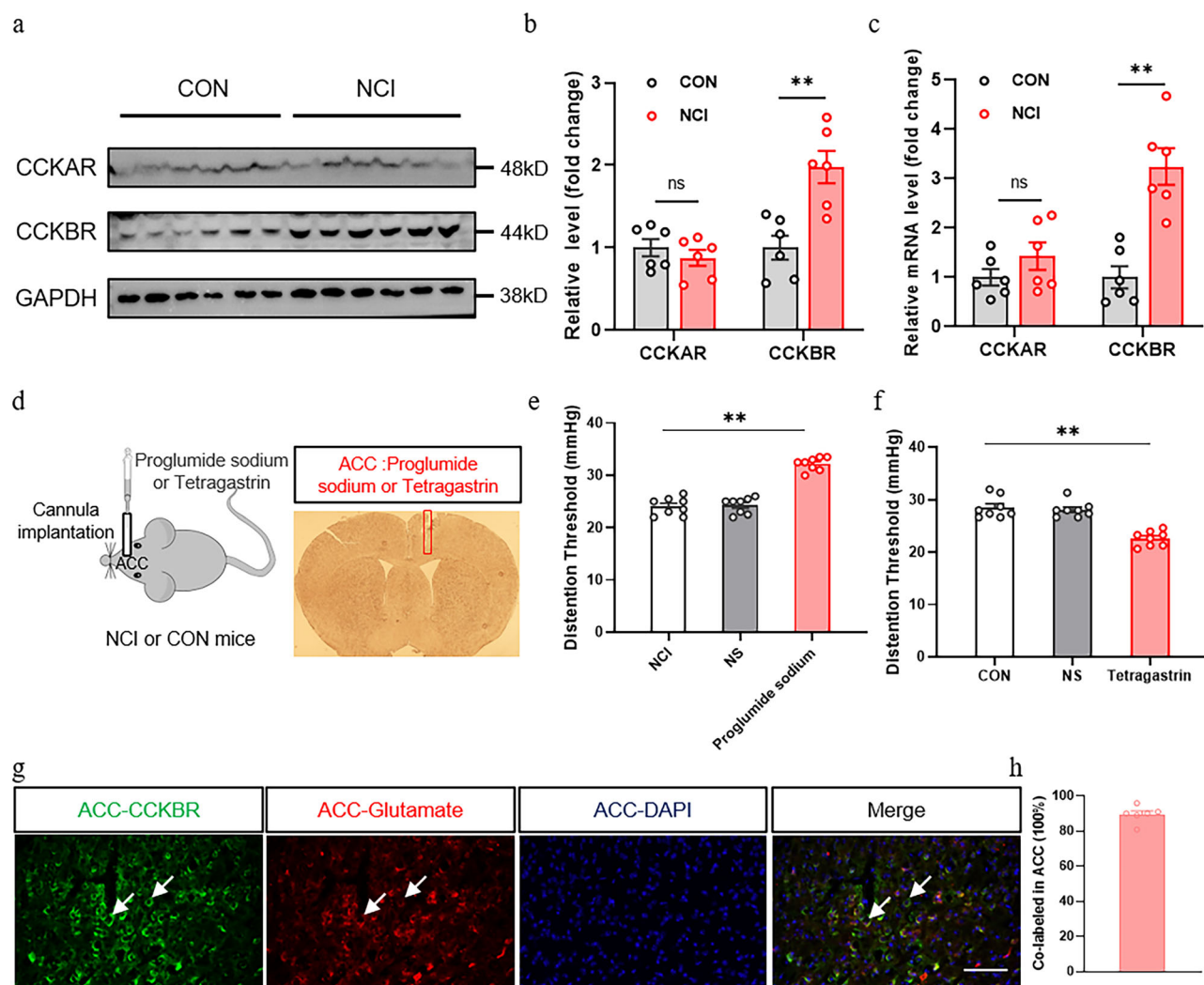


**Fig. 6 | ACC expression of CCKBRs is increased in NCI mice.** **a** Representative western blot of CCKAR and CCKBR expression in the ACC. **b** CCKBR receptor expression was significantly greater in the ACC of NCI mice than in that of CON mice ( $n = 6$  mice/group,  $p = 0.0002$ ). **c** The mRNA level of CCKBRs was markedly greater in the ACC of NCI mice than in that of CON mice ( $n = 6$  mice/group,  $p < 0.0001$ ). **d** Schematic of proglumide sodium or tetragastrin injection (left), and the red boxes show the site of microinjection into the ACC (right). **e** Bar plot showing the colorectal distension (CRD) threshold in NCI mice treated with proglumide sodium compared with those in the NCI and NS groups ( $n = 8$  mice/group,

$p < 0.0001$ ). **f** Bar plot showing the CRD threshold in CON mice treated with tetragastrin compared with those in the CON and NS groups ( $n = 8$  mice/group,  $p < 0.0001$ ). **g** Representative images showing the colocalization of CCKBR (green) and glutamatergic neurons (red) in the ACC of NCI mice. Scale bar: 20  $\mu$ m. **h** Percentage of colocalization in the ACC region ( $n = 3$  mice). All the data are presented as the means  $\pm$  SEMs. Two-way ANOVA with Sidak's multiple comparisons test (**b**, **c**). Ordinary one-way ANOVA with Dunnett's multiple comparisons test (**e**, **f**). \*\* $p < 0.01$ .

preference<sup>25</sup>. Combining with the previous studies, we speculate that the animals experiencing chronic visceral pain may exhibit reduced appetite or anhedonia, or may shift food preferences towards less palatable or less energy-dense options, potentially due to an altered dopaminergic signaling in the brain<sup>44</sup>. Although we did not investigate the effect of sucrose intake on the visceral pain threshold, our results revealed a role for cholecystokinin neurons and glutamatergic neurons signaling pathway in the brain.

A limitation of this study was that the experiments were performed solely in male mice; therefore, the results may not be entirely applicable to female mice. However, previous studies have shown that estrogen has an important effect on chronic pain<sup>45,46</sup>. Therefore, male animals were uniformly selected to exclude the effects of estrogen<sup>47,48</sup>. In this study, the calorie of intralipid (0.15 kcal/ml) is slightly higher than the calorie of sucrose (0.44 kcal/ml). In consideration of the reward effect of high sucrose solution<sup>49</sup> and the negative metabolic effects of high fat diet<sup>50</sup>, we chose 1% sucrose and 1.5% intralipid,

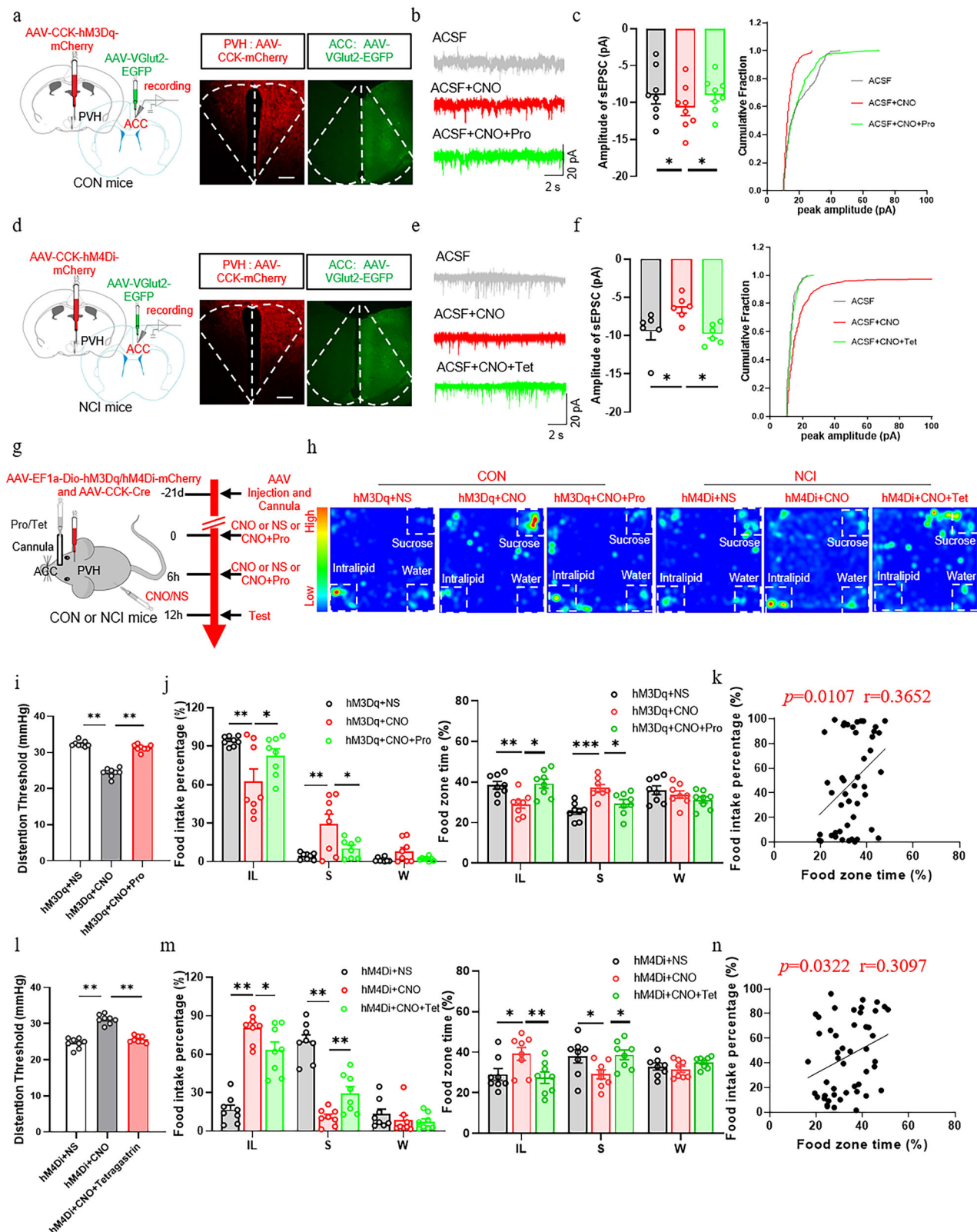
respectively. unequal calorie density of the intralipid and sucrose solution may affect the interpretation of our results. However, the use of inappropriate concentration may significantly change the taste of the food and thus affect the test of preference. As such, we chose these concentrations based on a study with the similar paradigm<sup>20</sup>.

In conclusion, the PVH<sup>CCK</sup>-ACC<sup>Glut</sup> neural circuit plays a role in regulating visceral pain and related changes in food preference. CCKBRs play significant roles in this process. Thus, targeting this circuit may be a potential approach for the clinical management of patients with chronic visceral pain.

## Methods

### Mice

Adult male and female mice aged 8–10 weeks (C57BL/6J and VGlut2-ires-Cre, respectively) were used for breeding. Each litter size has ranges from 4–6 pups. C57BL/6J mice were purchased from Shanghai SLAC Laboratory Animal Company, Ltd. The VGlut2-Cre mice were



purchased from Shanghai Model Organisms. A mouse model of chronic visceral pain was induced by NCI<sup>51,52</sup>. The mice had free access to water and food at a stable environment (23–25 °C, 40 to 60% relative humidity, and 12/ 12-h light/dark cycle). The handling of the animals was approved by the Soochow University Institutional Animal Care and Use Committee and was carried out in strict accordance with the guidelines of the International Association for the Study of Pain.

Given that estrogen synthesized in female mice may affect visceral pain<sup>53,54</sup>, adult female mice were excluded.

### Measurement of chronic visceral pain

Chronic visceral hypersensitivity was induced by NCI<sup>7</sup>. NCI modeling was performed on postnatal day 10. A homemade rectal injector was used to inject 0.5% acetic acid (prepared using physiological saline)



**Fig. 7 | CCKBRs mediate the regulatory role of the PVH<sup>CCK</sup>-ACC<sup>Glu</sup> circuit in chronic visceral pain-induced food preference changes.** **a** Schematic of chemogenetics manipulation and representative images of viral expression in the PVH and ACC. Scale bar: 20  $\mu$ m. **b** Representative traces of sEPSCs in ACC neurons following bath application of ACSF, CNO and then CNO with proglumide sodium. **c** Cumulative fraction plots and quantification of sEPSCs peak amplitude ( $n = 8$  cells/group, Pre vs CNO,  $p = 0.0114$ ; CNO vs CNO+Pro,  $p = 0.0121$ ). **d** Schematic of chemogenetic manipulation and representative images of viral expression in the PVH and ACC. Scale bar: 20  $\mu$ m. **e** Representative traces of sEPSCs in ACC neurons following bath application of ACSF or CNO, and subsequent application of CNO with tetragastrin. **f** Cumulative fraction plots and quantification of sEPSCs peak amplitude ( $n = 6$  cells/group, Pre vs CNO,  $p = 0.0447$ ; CNO vs CNO+Tet,  $p = 0.0252$ ). **g** Schematic of chemogenetic manipulation (left) and related experimental protocol (right). **h** Heatmaps of mouse location during the free-feeding tests. **i** Colorectal distension (CRD) thresholds following hM3Dq+NS, hM3Dq+CNO or

hM3Dq+CNO+proglumide sodium administration to CON mice ( $n = 8$  mice/group,  $p < 0.0001$ ). **j** Food zone time percentage and food intake percentage following hM3Dq+NS, hM3Dq+CNO or hM3Dq+CNO+proglumide sodium administration to CON mice ( $n = 8$  mice/group, Food intake percentage:  $p < 0.05$ ; Food zone time:  $p < 0.05$ ). **k** Correlation analysis between food zone percentage time and food intake percentage ( $p = 0.0107$ ,  $r = 0.3652$ ). **l** CRD threshold following hM4Di+NS, hM4Di+CNO or hM4Di+CNO+tetragastrin administration to NCI mice ( $n = 8$  mice/group,  $p < 0.0001$ ). **m** Food zone time percentage and food intake percentage following hM4Di+NS, hM4Di+CNO or hM4Di+CNO+tetragastrin administration to NCI mice ( $n = 8$  mice/group, Food intake percentage:  $p < 0.05$ ; Food zone time:  $p < 0.05$ ). **n** Correlation between the percentage of food zone time and percentage of food intake ( $p = 0.0322$ ,  $r = 0.3097$ ). All the data are presented as the means  $\pm$  SEMs. Two-way ANOVA with Sidak's multiple comparisons test (**j**, **m**). Ordinary one-way with ANOVA Tukey's multiple comparisons test (**c**, **f**, **i**, **l**). Linear regression and Correlation (**k**, **n**). \* $p < 0.05$ ; \*\* $p < 0.01$ ; \*\*\* $p < 0.001$ .

at a distance of 1 cm from the anus into the colorectum, with each mouse receiving an injection of 30  $\mu$ L. The CON group received an equivalent volume of medical-grade saline injected into the colorectum<sup>6</sup>. Briefly, a 2-cm balloon was inserted into the rectum through the anus after the mice were anesthetized with isoflurane. The balloon was attached to a polyethylene tube. The tube was secured by taping onto the tail. After 30 min of recovery, the mice were tested for pain using the CRD. The CRD threshold (mmHg) was recorded using a sphygmomanometer in a blinded manner by quickly inflating the balloon until an obvious abdominal withdrawal reflex was observed. The measurement was repeated 5 times at 3-min intervals, and the average CRD threshold was calculated.

## Diet

To explore the food preference in chronic visceral pain mice, we chose three food solution include intralipid (HY-131370B, MCE), sucrose and water. Intralipid is a mixture and effective in protecting the heart against ischemia-reperfusion injury and has some potential to modulate the innate immune response<sup>55</sup>. It is also a safe fat emulsion that can be used as a dietary supplement. In this experiment, we diluted its concentration to 1.5% and used it as a nutritional supplement. In consideration of the reward effect of high sucrose solution, we chose 1% sucrose<sup>49</sup> in our study. The water has not treatment.

## Food preference experiment

Mice were given ad libitum access to food and water for several days prior to the behavioral tests; any food or water restriction would severely affect the mice's behavior in preference. Development of food preference: the preference switch experiments were carried out in an open box (50 cm  $\times$  50 cm  $\times$  50 cm) and placed 1.5% intralipid, 1% sucrose, and water in three corners of the box. Mice were food and water deprived 8 h before the experiment and had ad libitum access to food throughout.

For food preference tests, to familiarize animals with the environment, the mice used test were placed in box for 20 min a day for 2 days before experiment test. Animals were tested for their food preference over 1 h. Based on the study<sup>56</sup> and our pilot experiments, we chose 1 hour time period devoted to food preference behavior because the food consumption patterns were stable within this time frame. Food was weighed before and after the test to calculate the food intake of the mice over the 1 h test period. Pre= weight of food prior to behavior test. Post= weight of food at the end of the behavior. Difference value between Pre and Post as the food consumption. Food intake percentage: the consumption of each food divided by the total number consumption of three food consumed. Animal movement was recorded using a video tracking system and the AnyMaze software, which recorded the time spent in the three corners with food. The percentage of time spent in the food area was calculated as follows: time spent in each food area divided by the

total time of three food areas. After each test, the area was cleaned with 75% ethanol. The aim is to prevent residual animal odor from affecting the experimental results.

## Slice electrophysiology

The mice (24–28 g) were euthanized after deep anesthesia with isoflurane, and brain slice electrophysiology was performed<sup>57</sup>. The brain was rapidly resected and placed in 32 °C oxygenated artificial cerebrospinal fluid (ACSF) with the following composition (in mM): 95 NaCl, 1.8 KCl, 1.2 KH<sub>2</sub>PO<sub>4</sub>, 7 MgSO<sub>4</sub>, 0.5 CaCl<sub>2</sub>, 26 NaHCO<sub>3</sub>, 15 glucose, and 50 sucrose. The solution pH was 7.3–7.4, and osmolarity of 310–320 mOsm. The brain was cut into 300  $\mu$ m thick coronal slices using a vibrating microtome (Leica, VT1200S, Germany), transferred into ACSF solution and stored at 32 °C until use. After pre-incubation for 1 h<sup>58</sup>, the slices were continuously perfused with oxygenated recording solution at a rate of 10–15 ml/min at room temperature. The composition of the recording solution was as follows (in mM): 127 NaCl, 1.8 KCl, 1.2 KH<sub>2</sub>PO<sub>4</sub>, 2.4 CaCl<sub>2</sub>, 1.3 MgSO<sub>4</sub>, 26 NaHCO<sub>3</sub>, and 15 glucose. The solution pH was 7.3–7.4, and the osmolarity was 300–310 mOsm. Neurons were visualized using infrared differential interference contrast video microscopy with a 40 $\times$  magnification water-immersion objective (BX51WI, Olympus, Japan). Whole-cell patch-clamp recordings were obtained from the visually identified ACC and PVH neurons. Patch pipettes were prepared using a puller (Sutter-P97, United States). The internal solution for recording action potentials and sEPSCs contained (in mM) the following: 133 K-glucuronate, 8 NaCl, 0.6 EGTA, 10 HEPES, 2Mg-ATP, and 0.3 Na-GTP. The pH was 7.2–7.4, and the osmolarity was 280–290 mOsm/kg. After G $\Omega$  seals (usually  $> 4$  G $\Omega$ ) were formed and the whole-cell configuration was obtained, neurons were tested to ensure that the resting membrane potential was more negative than  $-50$  mV and that direct depolarizing current injections evoked action potentials overshooting 0 mV. Data were acquired using a Digidata1440A interface, a Multiclamp 700 B amplifier, and the pClamp10 software. Data were sampled and filtered at 10 kHz using the Bessel filter of the amplifier. To ensure high-quality recordings, the series resistance ( $< 20$  M $\Omega$ ) was checked using the membrane test function of the pClamp10 software throughout the experiment. Data were stored on a computer and analyzed offline.

## Immunofluorescence staining

To detect CRD-induced c-Fos expression, the balloon was inflated to a pressure of 60 mmHg for a 20-s stimulation period, followed by a 3-min rest. Each mouse was subjected to five CRD stimulations. At 1 h after CRD stimulation, the mice were deeply anesthetized, and transcardial perfusion was performed with 0.9% physiological saline and 4% paraformaldehyde (PFA). Mouse brains were removed and post-fixed in PFA for 3–4 h. The brains were then treated with sucrose at concentrations of 10%, 20%, or 30%. This process continued until the brain tissue sank to the bottom of the sucrose solution. The brains were

sliced into 30- $\mu$ m coronal sections using a freezing microtome (Leica, Germany). The sections were incubated with 0.3% Triton X-100 for 1 h and blocked with 7% donkey serum for 1 h at room temperature.

They were then incubated with primary antibodies, including anti-c-Fos (1:100, rabbit, 9F6, Cell Signaling), anti-glutamate (1:100, mouse, G9282, Sigma), anti-CCK (1:100, mouse, Proteintech, PA5-103116) for 12 h at 4 °C. Following primary antibody incubation, the sections were incubated with the corresponding fluorophore-conjugated secondary antibodies (anti-rabbit Alexa Fluor 488, 1:500, A21206, Invitrogen and anti-mouse Alexa Fluor 555, 1:100, A31570, Invitrogen) at room temperature for 1 h. Fluorescent signals were detected using a confocal microscope (LSM700; Zeiss, Germany), processed, and exported with Zen software (Zeiss, Germany)<sup>59,60</sup>. Sections from the same coordinates were analysed for each group, with one section of the brain being removed from each mouse.

### Western blotting

The mice were deeply anesthetized with isoflurane and sacrificed via cervical dislocation. PVH coordinates were determined according to Paxinos and Franklin's *The Mouse Brain* (4<sup>th</sup> edition, 2013). Using these coordinates, acute dissection of the PVH tissue was performed in ice-cold oxygenated fresh ACSF containing the following solutions (in mM): 130 NaCl, 5 KCl, 2 KH<sub>2</sub>PO<sub>4</sub>, 10 HEPES, 10 glucose, 6 MgSO<sub>4</sub>, and 1.5 CaCl<sub>2</sub>. The pH was 7.2, and the osmolarity was adjusted to 305 mM with sucrose. After the PVH protein extracts were separated on 4% and 10% polyacrylamide gels, the proteins were transferred onto polyvinylidene difluoride membranes. For the CCK receptors, the membranes were blocked in Tris-buffered saline (TBS) with a 5% dilution of nonfat milk powder at room temperature. The membranes were then incubated with an anti-CCKAR antibody (1:100, A16799, ABclonal) and an anti-CCKBR antibody (1:100, A14567, ABclonal) overnight at 4 °C in TBS containing 1% milk. After washing in TBS containing 0.5% Tween-20, the membranes were incubated with horseradish peroxidase-conjugated secondary antibodies in TBS containing 1% milk at room temperature. Band intensities were measured with ImageJ. The CCKARs and CCKBRs protein expression levels were normalized to those of GAPDH.

### Real-time quantitative polymerase chain reaction

Total RNAs were extracted from ACC in CON and NCI mice with TRIzol (Vazyme, R411-01). cDNA was synthesized from total RNA using a Reverse transcription kit (Yeasen, I1155ES60) following the supplier's instructions. The sequences of the primer pairs for CCKARs and CCKBRs used in quantitative polymerase chain reaction were as follows: (F) 50- CTGGAGATACGGTGCCATC-30 and (R) 50-TGTAAATGGGGTACGGAGTCA -30; (F) 50- ATCTGCCGACCACT GCAAG-30 and (R) 50- GGTAGGGGACCATAAGCAATCC-30; the sequence of the primer pairs for gapdh (as an internal control) used in quantitative polymerase chain reaction is as follows: (F) 50 - AGGTCTGGTGTGAACGGATTG -30 and (R) 50- GGGGTCGTTGAT GGCAACA -30

### Drug administration

For the behavioral experiments, proglumide sodium (30  $\mu$ M, 1  $\mu$ l, MCE) or tetragastrin (30  $\mu$ M, 1  $\mu$ l, MCE)<sup>23</sup> was stereotactically injected into the right side of the ACC. The mice were allowed to recover for at least 3–4 days postoperatively before the behavioral tests. CRD was performed before and 10 min after drug microinjection. All drug concentrations used were based on a pilot study and previous studies<sup>61,62</sup>. The CNO injection methods included intraperitoneal injection and microinjection. Intraperitoneal injection of CNO at a dose of 0.33 mg/ml (0.2 ml) was used to investigate whether activation or inhibition of PVH neurons affected ACC neural activities and visceral pain responses<sup>63</sup>. Microinjection of CNO (0.33 mg/ml [1 ml]) into the ACC was used to examine whether proglumide sodium or tetragastrin

reversed the effect of CCK neuron terminals activation in the ACC on visceral pain responses<sup>64</sup>.

### Virus injection

During viral injection, the mice were preoperatively anesthetized with isoflurane and fixed in a stereotactic frame (RWD, 71000-M, Shenzhen, China). A heated blanket was used to maintain the body temperature at 36 °C. A volume of 200 nl of virus (depending on the viral titer) was injected at a rate of 20 nl/min using calibrated glass microelectrodes connected to an infusion pump (RWD, Shenzhen, China). The coordinates were defined as dorsal-ventral (DV) from the brain surface, anterior-posterior (AP) from the bregma, and mediolateral (ML) from the midline (mm). At each injection site, the micropipette was left in situ for 10 min after the completion of the injection to allow the viralspread and was subsequently withdrawn slowly.

For fiber photometry, 200 nl AAV2/9-CCK-GCaMP6f-EGFP or AAV2/9-VGlut2-GCaMP6f-EGFP was injected into PVH (AP: -0.6 mm, ML: +0.2 mm, DV: 4.6 mm) and ACC (AP: +1.0 mm, ML: -0.4 mm, DV: 2.0 mm).

For anterograde tracing, AAV2/9-hSyn-EGFP was injected into the right PVH of C57BL/6J mice. For retrograde tracing, AAV2/9-hSyn-EGFP was injected into the right ACC of C57BL/6J mice, and the virus spread in a retrogradely manner to the PVH soma to express GFP. For retrograde tracing, AAV-EF1a-DIO-TVA-GFP and AAV-EF1a-DIO-RVG were infused into the ACC. The EnvA-pseudotyped RV- $\Delta$ G-DsRed RV was injected into the same site into VGlut2-Cre mice 3 weeks later.

For CCK neurons in the PVH, viruses under the control of a cell-specific CCK promoter were used. AAV2/9-CCK-CRE and AAV2/9-EF1a-DIO-hm3Dq-mCherry viruses were used to activate the CCK neurons in CON mice. AAV2/9-CCK-CRE and AAV2/9-EF1a-DIO-hm4Di-mCherry were used to inhibit CCK neurons in the NCI mice. For glutamatergic neurons in the ACC, AAV2/9-VGlut2-hm3Dq-mCherry and AAV2/9-VGlut2-hm4Di-mCherry were used to label glutamatergic neurons in the ACC. After the mCherry protein was expressed for 3 weeks, CNO (2.5 mg/kg, BrainVTA, Wuhan, China) was intraperitoneally injected 1 h before the behavioral test. Unless otherwise stated, all viruses were packaged in BrainVTA (Wuhan, P. R. China). All the experiments were performed according to this protocol unless otherwise stated. In all experiments performed, the mice were excluded from the study if the viruses were injected into wrong coordinate or the optical fibers were implanted into wrong coordinate.

### Fiber photometry system

To evaluate the neuronal activity of the CCK and glutamatergic neurons, AAV2/9-CCK-GCaMP6f-EGFP or AAV2/9-VGlut2-GCaMP6f-EGFP were injected into PVH and ACC regions of the C57BL/6J mice. The fiber photometry (ThinkerTech Nanjing Biotech) was utilized to record calcium activity in the PVH (AP: -0.6 mm, ML: +0.2 mm, DV: 4.5 mm) and ACC (AP: +1.0 mm, ML: -0.4 mm, DV: 1.9 mm) 3 weeks after virus injection. Detection methods were the same as described earlier<sup>30</sup> and were briefly described below. A 488-nm laser beam was reflected off a dichroic mirror, focused with a 10x objective lens, and coupled to an optical commutator to record the calcium signals. The commutator and implanted fiber were connected by a 2-m optical fiber (200 mm O.D., 0.37 NA). The laser power was adjusted at the tip of the optical fiber to 10–20 mW to decrease laser bleaching, and the analog voltage signals were digitalized at 100 Hz and recorded by the fiber photometry system. The recording of the responses of GCaMP to the stimuli in awake mice was performed using fluorescence values obtained during the assessment by CRD. The data were segmented based on the behavioral events within the individual trials.  $\Delta F/F$  of the 2-s before stimulation was obtained as the baseline. The photometry data were analyzed with custom-written MATLAB codes (MATLAB R2017b, MathWorks).

## Statistical analyses

Data were reported as the mean  $\pm$  standard error of the mean (SEM), and the normality of data distribution was checked before all comparisons. Animals with incorrect viral microinjection or optic fiber placement were excluded from the analysis. The representative experiments results (such as micrographs) were independently repeated three times, with similar results obtained each time. Significance levels were indicated at  $*p < 0.05$ ,  $**p < 0.01$ , and  $***p < 0.001$ . Data were analyzed using a two-sample t-test, Mann–Whitney U-test, paired-sample t-test, unpaired-sample t-test, one-way repeated-measures ANOVA followed by Tukey's post hoc test, Dunn's post hoc test following Friedman ANOVA, and the Kolmogorov–Smirnov test, as appropriate. All statistical analyses were performed using GraphPad Prism 8.0 software (GraphPad Software, San Diego, CA, USA).

## Reporting summary

Further information on research design is available in the Nature Portfolio Reporting Summary linked to this article.

## Data availability

There are no restrictions on data availability in this manuscript. The data generated in this study are provided in the Source Data file. Source data are provided with this paper.

## References

- Elsenbruch, S., Häuser, W. & Jänig, W. Visceral pain. *Schmerz (Berl., Ger.)* **29**, 496–502 (2015).
- Zamyad, M., Abbasnejad, M., Esmaeili-Mahani, S., Sheibani, V. & Raoof, M. Pain influences food preference and food-related memory by activating the basolateral amygdala in rats. *Exp. Brain Res.* **239**, 79–93 (2021).
- Diogo, M. A., Ribas, G. G. & Skare, T. L. Frequency of pain and eating disorders among professional and amateur dancers. *Sao Paulo Med. J.* **134**, 0 (2016).
- Ciwoniuk, N., Wayda-Zaleska, M. & Kucharska, K. Distorted Body Image and Mental Pain in Anorexia Nervosa. *Int. J. Environ. Res. Public Health* **20**, 718 (2022).
- Verbanac, D., Maleš, Ž. & Barišić, K. Nutrition - facts and myths. *Acta Pharm. (Zagreb, Croat.)* **69**, 497–510 (2019).
- Zhang, F. C. et al. Paraventricular thalamus-insular cortex circuit mediates colorectal visceral pain induced by neonatal colonic inflammation in mice. *CNS Neurosci. Ther.* **30**, e14534 (2024).
- Wu, Y. Y., Wang, Q., Zhang, P. A., Zhu, C. & Xu, G. Y. miR-1306-3p directly activates P2X3 receptors in primary sensory neurons to induce visceral pain in rats. *Pain* **164**, 1555–1565 (2023).
- Xu, Q. Y. et al. Identification of a glutamatergic claustrum-anterior cingulate cortex circuit for visceral pain processing. *J. Neurosci. J. Soc. Neurosci.* **42**, 8154–8168 (2022).
- Wei, H. R. et al. A microglial activation cascade across cortical regions underlies secondary mechanical hypersensitivity to amputation. *Cell Rep.* **43**, 113804 (2024).
- Ntamat, N. R., Acuña, M. A. & Nevian, T. Pain-induced adaptations in the claustrum-cingulate pathway. *Cell Rep.* **42**, 112506 (2023).
- Smith, M. L., Asada, N. & Malenka, R. C. Anterior cingulate inputs to nucleus accumbens control the social transfer of pain and analgesia. *Sci. (N. Y., N. Y.)* **371**, 153–159 (2021).
- Wang, D. et al. Lateral septum-lateral hypothalamus circuit dysfunction in comorbid pain and anxiety. *Mol. psychiatry* **28**, 1090–1100 (2023).
- Liu, Y. et al. Oxytocin promotes prefrontal population activity via the PVN-PFC pathway to regulate pain. *Neuron* **111**, 1795–1811.e1797 (2023).
- Senba, E., Matsunaga, K., Tohyama, M. & Noguchi, K. Stress-induced c-fos expression in the rat brain: activation mechanism of sympathetic pathway. *Brain Res. Bull.* **31**, 329–344 (1993).
- Zhang, J. et al. Natural products and derivatives for breast cancer treatment: From drug discovery to molecular mechanism. *Phyto-medicine: Int. J. Phytother. Phytopharm.* **129**, 155600 (2024).
- Li, X. H. et al. Oxytocin in the anterior cingulate cortex attenuates neuropathic pain and emotional anxiety by inhibiting presynaptic long-term potentiation. *Cell Rep.* **36**, 109411 (2021).
- Atasoy, D., Betley, J. N., Su, H. H. & Sternson, S. M. Deconstruction of a neural circuit for hunger. *Nature* **488**, 172–177 (2012).
- Tang, H. D. et al. A neural circuit for the suppression of feeding under persistent pain. *Nat. Metab.* **4**, 1746–1755 (2022).
- Wank, S. A. Cholecystokinin receptors. *Am. J. Physiol.* **269**, G628–G646 (1995).
- Li, M. et al. Gut-brain circuits for fat preference. *Nature* **610**, 722–730 (2022).
- Greenberg, M. E., Ziff, E. B. & Greene, L. A. Stimulation of neuronal acetylcholine receptors induces rapid gene transcription. *Sci. (N. Y., N. Y.)* **234**, 80–83 (1986).
- Hou, Y. et al. Coordinated activity of a central pathway drives associative opioid analgesic tolerance. *Sci. Adv.* **9**, eabo5627 (2023).
- Zhang, N. et al. Cholecystokinin B receptor agonists alleviates anterograde amnesia in cholecystokinin-deficient and aged Alzheimer's disease mice. *Alzheimer's. Res. Ther.* **16**, 109 (2024).
- Berthoud, H. R., Morrison, C. D., Ackroff, K. & Sclafani, A. Learning of food preferences: mechanisms and implications for obesity & metabolic diseases. *Int. J. Obes.* **45**, 2156–2168 (2021).
- Tan, H. E. et al. The gut-brain axis mediates sugar preference. *Nature* **580**, 511–516 (2020).
- Ip, C. K. et al. Critical role of lateral habenula circuits in the control of stress-induced palatable food consumption. *Neuron* **111**, 2583–2600.e2586 (2023).
- Varela, L. & Horvath, T. L. Parallel paths in PVH control of feeding. *Neuron* **102**, 514–516 (2019).
- Xu, Y. et al. Lateral septum as a melanocortin downstream site in obesity development. *Cell Rep.* **42**, 112502 (2023).
- Qian, S. et al. A temperature-regulated circuit for feeding behavior. *Nat. Commun.* **13**, 4229 (2022).
- Li, Y. C., Wang, Q., Li, M. G., Hu, S. F. & Xu, G. Y. A paraventricular hypothalamic nucleus input to ventral of lateral septal nucleus controls chronic visceral pain. *Pain* **164**, 625–637 (2023).
- Fukushima, A., Kataoka, N. & Nakamura, K. An oxytocinergic neural pathway that stimulates thermogenic and cardiac sympathetic outflow. *Cell Rep.* **40**, 111380 (2022).
- Chen, C. R. et al. Dysfunctions of the paraventricular hypothalamic nucleus induce hypersomnia in mice. *eLife* **10**, e69909 (2021).
- Liu, Y. et al. Distinct hypothalamic paraventricular nucleus inputs to the cingulate cortex and paraventricular thalamic nucleus modulate anxiety and arousal. *Front. Pharmacol.* **13**, 814623 (2022).
- Guo, B. et al. CB1R dysfunction of inhibitory synapses in the ACC drives chronic social isolation stress-induced social impairments in male mice. *Neuron* **112**, 441–457.e446 (2024).
- Song, Q. et al. An ACC-VTA-ACC positive-feedback loop mediates the persistence of neuropathic pain and emotional consequences. *Nat. Neurosci.* **27**, 272–285 (2024).
- Li, X. H. et al. Activation of the glutamatergic cingulate cortical-cortical connection facilitates pain in adult mice. *Commun. Biol.* **6**, 1247 (2023).
- Zhu, X. et al. Distinct thalamocortical circuits underlie allodynia induced by tissue injury and by depression-like states. *Nat. Neurosci.* **24**, 542–553 (2021).
- Funakoshi, A. Cholecystokinin and cholecystokinin receptor]. *Nihon rinsho. Jpn. J. Clin. Med.* **54**, 1097–1103 (1996).
- Takemi, S. et al. Molecular cloning of cholecystokinin (CCK) and CCK-A receptor and mechanism of CCK-induced gastrointestinal



- motility in *Suncus murinus*. *Gen. Comp. Endocrinol.* **327**, 114074 (2022).
40. Zhang, X. et al. Cholecystokinin B receptor antagonists for the treatment of depression via blocking long-term potentiation in the basolateral amygdala. *Mol. psychiatry* **28**, 3459–3474 (2023).
  41. Zhang, J. F. et al. Potential molecular mechanisms of electroacupuncture with spatial learning and memory impairment induced by chronic pain on a rat model. *Pain. physician* **25**, E271–e283 (2022).
  42. Nuseir, K. Q., Altarifi, A. Y., Tasslaq, A., Alhusban, A. Y. & Alzoubi, K. H. Early and late anti nociceptive effects of sucrose on neonatal inflammatory pain in rats: comparison to a non-steroidal anti-inflammatory drug. *Physiol. Behav.* **206**, 37–42 (2019).
  43. Thambireddy, S., Svsg, N. & Nuvvula, S. Sucrose solution for alleviating needle pain during inferior alveolar nerve block in children aged 7–10 years: a randomized clinical trial. *J. Dent. anesthesia pain. Med.* **23**, 273–280 (2023).
  44. Land, B. B. et al. Medial prefrontal D1 dopamine neurons control food intake. *Nat. Neurosci.* **17**, 248–253 (2014).
  45. Lee, J. et al. Estrogen mediates the sexual dimorphism of GT1b-induced central pain sensitization. *Cells* **12**, 808 (2023).
  46. Xu, X. et al. GPR30-mediated non-classic estrogen pathway in mast cells participates in endometriosis pain via the production of FGF2. *Front. Immunol.* **14**, 1106771 (2023).
  47. Sun, L. H. et al. Estrogen modulation of visceral pain. *J. Zhejiang Univ. Sci. B* **20**, 628–636 (2019).
  48. Swanson, K. A., Nguyen, K. L., Gupta, S., Ricard, J. & Bethea, J. R. TNFR1/p38 $\alpha$ MAPK signaling in Nex + supraspinal neurons regulates estrogen-dependent chronic neuropathic pain. *Brain, Behav., Immun.* **119**, 261–271 (2024).
  49. Ren, J. N. et al. Effect of short-term intake of high- and low-concentrations of sucrose solution on the neurochemistry of male and female mice. *Food Funct.* **11**, 9103–9113 (2020).
  50. Lee, J. H. et al. Heat-killed enterococcus faecalis prevents adipogenesis and high fat diet-induced obesity by inhibition of lipid accumulation through inhibiting C/EBP- $\alpha$  and PPAR- $\gamma$  in the insulin signaling pathway. *Nutrients* **14**, 1308 (2022).
  51. Wu, R. et al. Decreased miR-325-5p contributes to visceral hypersensitivity through post-transcriptional upregulation of CCL2 in rat dorsal root ganglia. *Neurosci. Bull.* **35**, 791–801 (2019).
  52. Wu, Y. Y. et al. Targeting GATA1 and p2x7r locus binding in spinal astrocytes suppresses chronic visceral pain by promoting DNA demethylation. *Neurosci. Bull.* **38**, 359–372 (2022).
  53. Mulak, A. & Taché, Y. Sex difference in irritable bowel syndrome: do gonadal hormones play a role? *Gastroenterol Pol.* **17**, 89–97 (2010).
  54. Sanoja, R. & Cervero, F. Estrogen-dependent changes in visceral afferent sensitivity. *Autonomic Neurosci.: basic Clin.* **153**, 84–89 (2010).
  55. Li, J. et al. Intralipid, a clinically safe compound, protects the heart against ischemia-reperfusion injury more efficiently than cyclosporine-A. *Anesthesiology* **117**, 836–846 (2012).
  56. Agee, L. A., Nemchek, V., Malone, C. A., Lee, H. J. & Monfils, M. H. Appetitive behavior in the social transmission of food preference paradigm predicts activation of orexin-A producing neurons in a sex-dependent manner. *Neuroscience* **481**, 30–46 (2022).
  57. Xiao, Y. et al. TRPV1-mediated presynaptic transmission in basolateral amygdala contributes to visceral hypersensitivity in adult rats with neonatal maternal deprivation. *Sci. Rep.* **6**, 29026 (2016).
  58. Zhang, P. A. et al. Neonatal maternal deprivation enhances presynaptic P2X7 receptor transmission in insular cortex in an adult rat model of visceral hypersensitivity. *CNS Neurosci. therapeutics* **23**, 145–154 (2017).
  59. Wang, H. et al. Incerta-thalamic circuit controls nociceptive behavior via cannabinoid type 1 receptors. *Neuron* **107**, 538–551.e537 (2020).
  60. Zhou, K. et al. Dual electrical stimulation at spinal-muscular interface reconstructs spinal sensorimotor circuits after spinal cord injury. *Nat. Commun.* **15**, 619 (2024).
  61. González-Puga, C. et al. Selective CCK-A but not CCK-B receptor antagonists inhibit HT-29 cell proliferation: synergism with pharmacological levels of melatonin. *J. pineal Res.* **39**, 243–250 (2005).
  62. Ahmad, M., Abu-Taweel, G. M., Aboshaiqah, A. E. & Ajarem, J. S. The effects of quinacrine, proglumide, and pentoxifylline on seizure activity, cognitive deficit, and oxidative stress in rat lithium-pilocarpine model of status epilepticus. *Oxid. Med. Cell. Longev.* **2014**, 630509 (2014).
  63. Yin, J. B. et al. dmPFC-vLPAG projection neurons contribute to pain threshold maintenance and antianxiety behaviors. *J. Clin. Investig.* **130**, 6555–6570 (2020).
  64. Chen, Y. H. et al. Distinct projections from the infralimbic cortex exert opposing effects in modulating anxiety and fear. *J. Clin. Invest.* **131**, e145692 (2021).

## Acknowledgements

This work was supported by grants from National Natural Science Foundation of China (82301401, 82302465, 82471281, and 82072130), Boxi Excellent Talent Casting Plan (Y.-F.Y.) and Boxi Incubation plan (Y.K.). Health Talent Plan Project in Suzhou (GSWS2022007). Key Medical Research Projects in Jiangsu Province (ZD2022021), Key R&D Program Projects in Jiangsu Province (BE2023709), Health Talent Plan Project in Suzhou (GSWS2022007), Suzhou Key Laboratory of Anesthesiology (SZS2023013), Suzhou Clinical Medical Center for Anesthesiology (Szlcycxj202102), and National Clinical Key Specialty for Anesthesiology. The funders had no role in the study design, data collection and analysis, decision to publish, or preparation of the manuscript.

## Author contributions

Q.-Y.X. performed experiments, analyzed data, and prepared figures and manuscript. Y.K. and X.-W.M. performed experiments and analyzed data. K.P. and Y.Y. performed most of edited the manuscript. S.-Y.S. and Y.-F.Y. performed experiments. H.-Y.L. analyzed data and edited the manuscript. F.-H.J. and G.-Y.X. designed and supervised the experiments and finalized the manuscript. All the authors have read and approved the paper.

## Competing interests

The author(s) declare no competing interests.

## Additional information

**Supplementary information** The online version contains supplementary material available at <https://doi.org/10.1038/s41467-025-61178-2>.

**Correspondence** and requests for materials should be addressed to Hua-Yue Liu, Guang-Yin Xu or Fu-Hai Ji.

**Peer review information** *Nature Communications* thanks Mehdi Abbasnejad, Zhi Zhang and the other, anonymous, reviewer(s) for their contribution to the peer review of this work. A peer review file is available.

**Reprints and permissions information** is available at <http://www.nature.com/reprints>

**Publisher's note** Springer Nature remains neutral with regard to jurisdictional claims in published maps and institutional affiliations.

**Open Access** This article is licensed under a Creative Commons Attribution-NonCommercial-NoDerivatives 4.0 International License, which permits any non-commercial use, sharing, distribution and reproduction in any medium or format, as long as you give appropriate credit to the original author(s) and the source, provide a link to the Creative Commons licence, and indicate if you modified the licensed material. You do not have permission under this licence to share adapted material derived from this article or parts of it. The images or other third party material in this article are included in the article's Creative Commons licence, unless indicated otherwise in a credit line to the material. If material is not included in the article's Creative Commons licence and your intended use is not permitted by statutory regulation or exceeds the permitted use, you will need to obtain permission directly from the copyright holder. To view a copy of this licence, visit <http://creativecommons.org/licenses/by-nc-nd/4.0/>.

© The Author(s) 2025